AN ABSTRACT OF THE THESIS OF

Rajarajan Senguttuvan for the degree of Master of Science in

Electrical and Computer Engineering presented on December 8, 2003.

Title:

Analysis and Modeling of Multi-mode Effects in Coplanar Waveguide Bends.

Redacted for privacy

Abstract approved: _____

Andreas Weisshaar

A novel method for modeling bends in coplanar waveguides (CPWs) is described. The CPW can be viewed as a pair of parallel coupled quasi-slot lines. Bends in the CPW are modeled as a non-uniform coupled line system in terms of their even- and odd- mode characteristics. This modeling approach is general and can be applied for bends with different angles and other similar discontinuities in the CPW. The salient feature of the model is the simplified illustration of frequency-dependent effects in the bend. Right-angle, 45 degree, and mitered right-angle bends in the CPW are analyzed, and models are developed for each bend structure. The procedure for extracting the modal scattering matrix from the model is presented. To demonstrate the accuracy of the model, modal transmission coefficients obtained from the model are compared with full-wave electromagnetic simulations. Good agreement between the model and full-wave simulation results over a wide frequency range is demonstrated.

The transfer of energy between even and odd modes in the bend is investigated and the effect of the physical properties of the CPW on mode conversion is analyzed in detail. Mode conversion at discontinuities like the bend in CPWs

cause non-ideal behavior in the two-port (even-mode) measurements of such circuits. Theoretical prediction of the measured response is discussed along with the predicted response for transmission coefficient from model and full-wave simulations. Comparison between the measurements of a right-angle bend and the corresponding model results shows good agreement. Implementation of the model in SPICE is also discussed.

Analysis and Modeling of Multi-mode Effects in Coplanar Waveguide Bends

by

Rajarajan Senguttuvan

A THESIS

submitted to

Oregon State University

in partial fulfillment of
the requirements for the
degree of

Master of Science

Presented December 8, 2003
Commencement June 2004

Master of Science thesis of Rajarajan Senguttuvan presented on December 8, 2003

APPROVED:

Redacted for privacy

Major Professor, representing Electrical and Computer Engineering

Redacted for privacy

Director of the School of Electrical Engineering and Computer Science

Redacted for privacy

Dean of the Graduate School

I understand that my thesis will become part of the permanent collection of Oregon State University libraries. My signature below authorizes release of my thesis to any reader upon request.

Redacted for privacy

Rajarajan Senguttuvan, Author

ACKNOWLEDGMENTS

First, I would like to thank my major professor, Dr.Andreas Weisshaar for having provided me with a great opportunity to pursue research at the Electrical engineering department. His unwavering support and guidance has been a source of inspiration during my graduate years at Oregon State University.

I would also like to thank Dr. Raghu Kumar Settaluri for the useful discussions that I have had with him. His lectures were a great learning experience.

Thanks to Cascade Microtech Inc. for the support towards my graduate research. I would like to thank Dr. Leonard Hayden at Cascade Microtech Inc. for serving as a faculty member in my graduate committee.

Thanks to Dr. Charles Brunner for serving as the Graduate Council Representative in my graduate committee and reviewing my manuscript.

I would also like to thank Dr. Gabor Temes, Dr. Terri Fiez, Dr. Un-ku Moon, and Dr. Wen-Tsong Shiue for their wonderful lectures.

Thanks to my colleagues, Amy Luoh, Harish Peddhibhotla, Sorwar Hossain, Yevgeniy Mayevisky, Adam Watson, Kala Gururajan, Chi-Young Lim, and Dan Melendy for their encouragement, useful discussions, and contributions to this work.

Thanks to Ferne Simendinger, April Melton, and the personnel at Graduate School for their help.

Special thanks to my parents, family and friends in India for their encouragement and support.

Finally, I would like to thank my friends in Corvallis for all their help.

TABLE OF CONTENTS

TABLE OF CONTENTS (Continued)

LIST OF FIGURES

LIST OF FIGURES (Continued)

Figure Page

ANALYSIS AND MODELING OF MULTI-MODE EFFECTS IN COPLANAR WAVEGUIDE BENDS

1. INTRODUCTION

1.1. Background and Motivation

The wires or transmission lines that are used to connect individual components in Integrated Circuits (ICs) and Printed Circuit Boards (PCBs), are commonly referred to as interconnects. They are attracting greater attention today in the design of integrated systems as their electrical behavior has become a limiting factor in system performance. In general, interconnects may cause signal delay, dispersion, power losses and interference with other parts of a circuit. These effects are more critical in high-speed, high-frequency systems with dense integration of components.

Interconnects are usually fabricated in various shapes of planar transmission lines. The different types include microstrips, striplines, slotlines, and coplanar waveguides (CPWs). CPW is a type of planar transmission line that has both the signal and ground conductors on the same side of the substrate. Figure 1.1 shows a typical CPW. It consists of a center strip of metal deposited on the surface of a substrate with two parallel strips on either side. The two strips on each side of the center conductor serve as ground lines and are assumed to be of infinite dimension laterally.

CPWs have gained increasing popularity in recent years over conventional transmission lines like the microstrip due to several advantages they offer for appli-

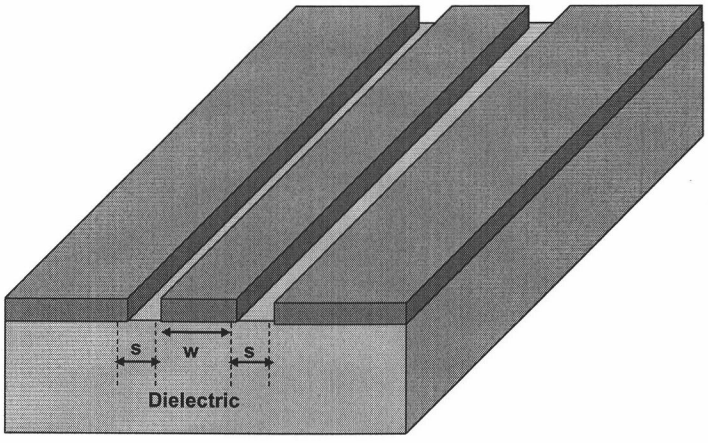

FIGURE 1.1. Coplanar Waveguide

cation in radio frequency (RF) and microwave circuits. Most important among them is the ease of manufacturability, connection of shunt elements, and their suitability for surface mount applications. There is no need to drill via holes, thus easing the fabrication and cost of CPW-based circuits. Furthermore, the characteristic impedance of the CPW is less sensitive to dielectric thickness compared to other common transmission lines. Impedance can be varied by changing the width and spacing of the conductors on one side of the substrate. This gives an additional degree of flexibility in the design of uniplanar circuits for RF/microwave applications. Other notable advantages of the CPW include low dispersion and dielectric losses [1], [2], and easy applicability to ferrite circuits [3].

In spite of their increasing popularity, there is a lack of comprehensive software tools for the design of CPW circuits. The reason for this is the shortage of models for common transmission line discontinuities like bends, T-junctions, line-transitions etc. This makes the design of CPW-based circuits difficult and time consuming. Figure 1.2 shows some typical coplanar discontinuities. As operating frequencies and device speeds continue to increase, it is becoming more critical to

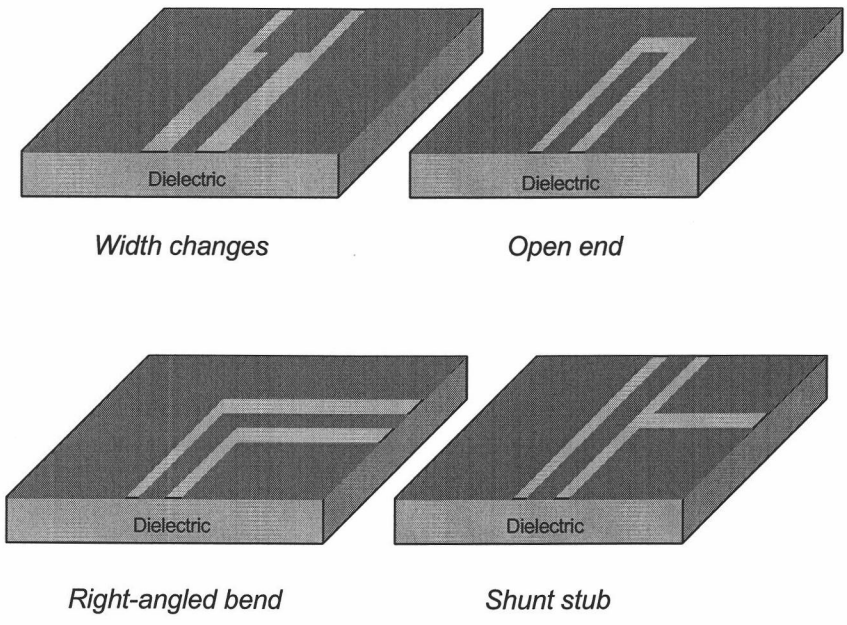

FIGURE 1.2. Typical Coplanar Waveguide Discontinuities

have a thorough understanding of the parasitic effects at discontinuities and to develop accurate characterization techniques.

Extensive research has been undertaken in the past years to characterize a variety of CPW discontinuities including transitions and discontinuities [4] - [23]. Most of the above mentioned work is based on full-wave electromagnetic (EM) analysis of the structures. The vector wave equation is solved for the electric and magnetic fields subject to boundary conditions. The parameters of the CPW can then be obtained from the field information. Typical techniques, which have been adopted for full-wave analysis, include Method of Moments (MoM), Finite Difference Time Domain Method (FDTD), Finite Element Method (FEM) etc. These methods produce accurate frequency-dependent characteristics of structures but tend to be complex and have long simulation times. The computation time can be reduced considerably

if a *quasistatic* approximation is used in the analysis. In quasistatic analysis, the spatial distribution of electric and magnetic fields is assumed to be nearly the same as for static fields. The calculation of line parameters is therefore reduced to a static field problem. The commonly used quasistatic methods include Spectral Domain Approach (SDA), Finite Difference Method (FDM) etc. SDA is one of the popular approaches for analyzing planar transmission line structures [24]. Application of SDA to characterize certain CPW discontinuities can be found in [25].

In general, EM simulations, whether full-wave or quasistatic, are time-consuming and require expensive computational resources. The use of EM solutions may be mandatory in applications that require a high degree of accuracy. But for most practical applications, the ease and speed of analysis outweighs accuracy considerations. In some cases, simple models can be derived for discontinuities using the geometry and cross-sectional information of the discontinuity. Equivalent circuit models, that can be used instead of EM solvers for fast analysis with sufficient degree of accuracy, are highly preferable. Moreover, if the discontinuity can be modeled using only ideal circuit elements, the equivalent circuit model can be implemented directly in time domain simulators like SPICE. One of the main motivations of this thesis is to therefore develop simple circuit models for bend discontinuities in CPWs.

There are two fundamental modes of propagation that exist in a CPW. They are the even and odd modes, excited by symmetric and anti-symmetric excitations, respectively. CPW-based circuits are normally operated in the even mode, but asymmetric discontinuities including bends, excite the odd mode and couple energy away from the even mode. This transfer of energy, referred to as mode conversion, is undesirable as power is lost from the desired mode-of-operation and can interfere with other parts of the circuit. Since the CPW is a two-mode structure, a four-port model would prove useful in the analysis of discontinuities. Four-port models

for discontinuities completely describe the system vis-a-vis the interaction between modes and therefore mode conversion.

Mode conversion at various discontinuities has been analyzed through full-wave simulations in [4] - [16]. Circuit models for mode-conversion in asymmetric discontinuities such as series and shunt stubs, and CPW-to-slot line transitions have been developed in [32] - [36]. A CPW right-angle bend is full-wave characterized in [4], and the effect of mode conversion on two-port measurements is discussed. In this thesis, a new four-port modeling approach is developed to analyze CPW bends. The model provides a quick and convenient way to observe the frequency-dependent effects of the bend with good accuracy. The effects of geometry of the bend discontinuity on mode conversion are studied in detail using this modeling approach, and the results are validated with full-wave simulations.

Mode conversion causes significant problems in the measurement of CPW-based structures. The connectors and devices connected to the CPW support only the even mode, forcing a symmetric condition at the terminations. The odd mode therefore gets reflected back-and-forth between the discontinuity and connectors. This can considerably complicate the calibration and measurement of such structures [30]. The measurement accuracy of CPW-based circuits is also affected by this excitation of the odd mode. A thorough understanding of multi-mode effects on single-mode two-port measurements is therefore needed. Characterization of mode conversion at the discontinuities in CPWs is a necessary requisite for predicting the actual measured response of the structure.

1.2. Organization of the Study

The focus of this thesis is to develop a modeling methodology that accounts for the frequency-dependent behavior of typical bends in the CPW. A novel approach

is presented here for modeling CPW bends of various angles and mitered bends. Models developed for bend discontinuities are based on the decomposition of the CPW as a pair of coupled quasi-slot lines. The effect of mode conversion on the measurement of CPW-based structures is also elucidated.

Chapter 2 presents the basic theory of CPW transmission lines. Past work on full-wave and quasistatic methods that have been used to study CPWs are mentioned. The latter part of the chapter dwells on the analysis and characterization of multi-conductor transmission lines. The study of multi-conductor transmission lines is important in this context, as the properties of CPWs are later derived based on multi-conductor transmission line theory. The technique adopted to find the line parameters of CPWs from the capacitance matrix of the corresponding 3-conductor system is given. Furthermore, typical discontinuities in CPWs are introduced along with the general approach that is used to characterize them.

Chapter 3 starts with a brief description of coupled line theory as a prelude to the model development for CPW bends. The similarities in transmission characteristics of CPWs and coupled quasi-slot lines are highlighted. Bends in the coplanar structure are then analyzed as non-uniform coupled quasi-slot lines. A generic four-port model for CPWs is presented based the non-uniform coupled quasi-slot lines. The procedure for extracting the modal scattering parameters from model results is given. In the latter part of the chapter, the modal transmission coefficients derived from the model are compared with those obtained from MOMENTUM [31] for right-angle, 45 degree and mitered bends. The comparisons have been done for different right-angle bends to study the effect of geometry and dielectric constant on the modes of the system.

Chapter 4 deals with the measurement of CPW-based structures. The basics of network analyzer measurements are discussed with an emphasis on the need for

calibration and the different techniques used. Multi-mode effects associated with right-angle CPW bend two-port measurements have been characterized. Theoretical results for the bend transmission coefficient S_{12} are derived from the respective model and MOMENTUM generated modal scattering parameters. A comparison between the actual measured response and model results is then given to demonstrate the validity of the model. Finally, implementation of the four-port model in SPICE [38] is described.

Chapter 5 summarizes the study and suggests areas for further research on the topic.

2. CPW TRANSMISSION LINES AND DISCONTINUITIES

2.1. Introduction

This chapter introduces the basic theory and analysis of CPW transmission lines. Multi-conductor transmission lines are then studied and a general theory for obtaining transmission line parameters for such structures is described. Next, an introduction is given to discontinuities in CPWs. A discontinuity is defined as any abrupt change in the structure that forces a change in field configuration of the propagating wave. Discontinuities in a CPW can be broadly classified as symmetric and asymmetric. Examples of symmetric discontinuities include the open stub, two-sided shunt stub etc. The asymmetric discontinuities on the other hand include bends, T-junctions and one-sided shunt stubs. The asymmetric discontinuities, by virtue of their geometry, excite the parasitic odd mode that deteriorates the performance of the system. The methodology adopted to analyze the effect of discontinuities, particularly mode conversion at asymmetric discontinuities, are discussed later in this chapter.

2.2. Analysis of Coplanar Transmission Lines

Figure 2.1 (a) shows the cross-section of a CPW. It is composed of three thin metallic films deposited on the surface of a substrate. The center strip is usually the signal conductor, and the other two conductors serve as the ground. CPW does not support a Transverse Electromagnetic (TEM) mode of transmission. TEM, as the name suggests, implies that the electric and magnetic fields are entirely transverse to the direction of propagation. The electric field between the center conductor

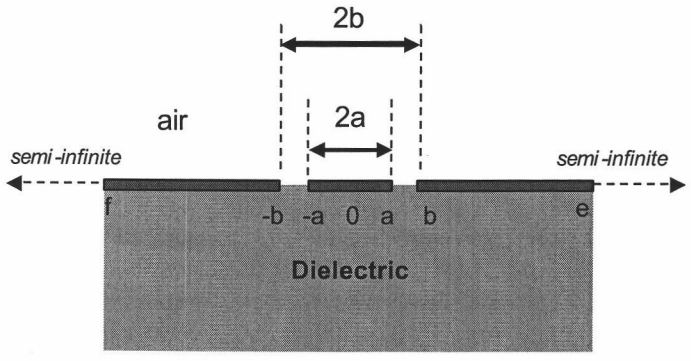

(a) CPW cross-section

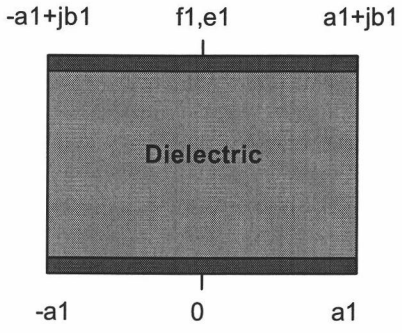

(b) Conformal transformation

FIGURE 2.1. CPW Crossection

and ground electrodes is tangential to the air-dielectric boundary. The tangential electric field configuration forces the axial and transverse components of magnetic field components, as discussed in [3].

Due to the growing popularity of CPWs over the past decades, considerable work has been undertaken to study coplanar waveguides. Wen [26] studied CPWs with the assumption that the dielectric substrate is thick enough to be considered infinite. This assumption makes it possible to apply techniques such as conformal-mapping to study the CPWs. Conformal transformation is a powerful analytical

technique, which can be used to simplify the analysis of planar transmission lines. The characteristic impedance has been calculated as a function of the ratio a/b, where $2a$ is the width of the center strip and $2b$ is the distance between the two ground planes. The dielectric half-plane is transformed to the interior of a rectangle in the complex plane using conformal techniques as shown in Fig 2.1 (b). The capacitance between the top and bottom plates of the rectangle is then given by

$$C = (\epsilon_r + 1)\epsilon_o \frac{2a1}{b1} \tag{2.1}$$

where the ratio a1/b1 is obtained from the transformation

$$\frac{a1}{b1} = \frac{K(k)}{K'(k)} \tag{2.2}$$

where

$$k = \frac{a}{b}$$

Here, K(k) is the complete elliptic integral of the first kind having the following property

$$K'(k) = K(k')$$

where

$$K'(k) = \frac{dK}{dk}$$

and

$$k' = (1 - k^2)^{1/2}$$

To calculate the phase velocity, the CPW is to be treated as a transmission line completely immersed in a homogenous dielectric [26] with effective dielectric constant ϵ_{eff}

$$\epsilon_{eff} = \frac{\epsilon_r + 1}{2} \tag{2.3}$$

Since a large fraction of electric fields for a CPW is in the air region, the effective dielectric constant for CPWs is usually lower than that for conventional transmission lines like microstrips on the same substrate. The phase velocity and characteristic impedance of the CPW are correspondingly given as

$$v_{ph} = \frac{c}{\sqrt{\epsilon_{eff}}} = c(\frac{2}{\epsilon_r + 1})^{1/2} \tag{2.4}$$

and

$$Z_o = \frac{v_{ph}}{C} \tag{2.5}$$

where

c is the velocity of light in free space and C is the capacitance per unit length of the CPW.

An important property of the CPW is the relative insensitivity of characteristic impedance to changes in substrate thickness. This property is more pronounced for substrates with higher relative dielectric constants. For example, it has been studied in [3] that the characteristic impedance changes by less than 10% when the thickness is reduced from infinity to about $(b-a)/2$ for a relatively large ϵ_r. This insensitivity of the CPW characteristic impedance gives an additional flexibility in the design of CPWs for RF circuits and integration with other components on the circuit board. Desired values of characteristic impedance can be obtained by just changing the a/b ratio for any substrate thickness.

The above mentioned values for phase velocity and characteristic impedance hold good for large values of ϵ_r and thick dielectrics, but do not approximate well the case of thin dielectrics and small ϵ_r. An alteration of the method used by Wen can be found in [28], where the finite thickness of the dielectric substrate has been taken

into account. Also, some applications require accurate frequency-dependent characterization of CPWs. Equations (2.1) - (2.3) have been obtained from quasistatic approximations, and hence, lack any frequency-dependent information. Extension of the analysis of CPWs to include the frequency-varying characteristic impedance and dispersion characteristics has been given in [27]. A hybrid-mode analysis is employed in [27] to study the CPW and extract the line parameters. For most practical transmission line problems though, the spatial distribution of the electric and magnetic fields are assumed constant though the actual fields may be time-varying. The characteristics of such structures can be obtained from quasistatic parameters derived from the solution of a static-field problem.

2.2.1. Multi-Conductor Structures

Multi-conductor structures are a common occurrence in practical field problems, and some powerful techniques have been developed to analyze and derive the line parameters of such systems. Once the line parameters like characteristic impedance, propagation constants, attenuation constants and the normal modes of propagation are derived, the system is completely described. The initial assumption for this analysis is that the transmission lines under consideration are ideal and the modes of propagation are purely TEM.

The dominant modes of propagation on the inhomogeneous lines are inherently non-TEM, but can be considered quasi-TEM at relatively low frequencies. As explained before, this approximation greatly simplifies the problem by making the application of static electromagnetic field analysis possible. This holds good with an accuracy of 1%, provided the substrate thickness is no greater than about 3% of the wavelength [29].

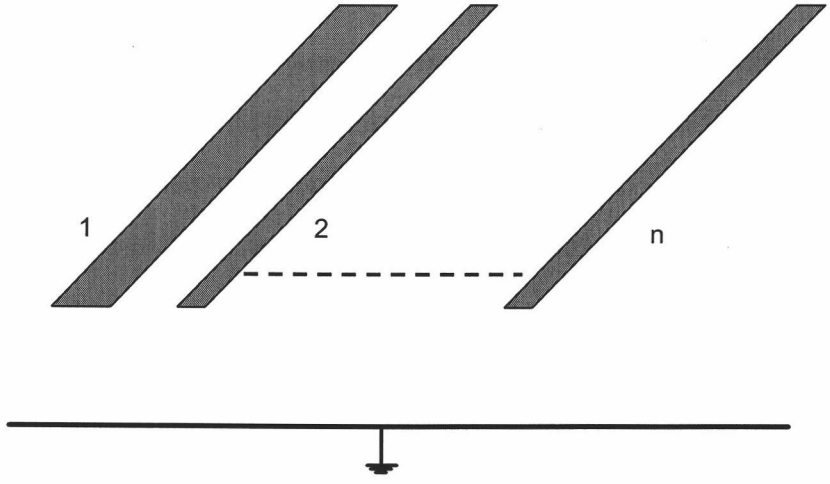

FIGURE 2.2. Multi-conductor system

Figure 2.2 shows a typical multi-conductor system. The line voltages and currents of such a system are represented as vectors, and the distributed capacitances and inductances are written in matrix form comprising the self and mutual terms. A detailed study of coupled transmission line systems is given in the next chapter. The incremental equivalent circuits for single and multiple coupled lines are shown in Figure 2.3. For a single transmission line described in Fig 2.3(a), the fundamental differential equations for voltage and current can be derived from simple circuit analysis as

$$\frac{\partial V}{\partial z} = -L\frac{\partial I}{\partial t} \tag{2.6}$$

$$\frac{\partial I}{\partial z} = -C\frac{\partial V}{\partial t} \tag{2.7}$$

where L is the distributed inductance of the line per unit length, and C is the distributed capacitance between the lines per unit length. The above equations for

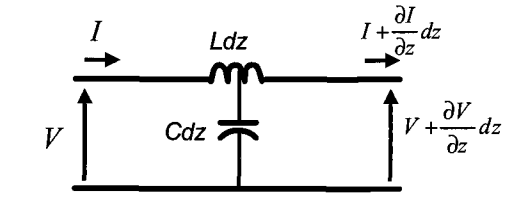

(a) Single Transmission Line

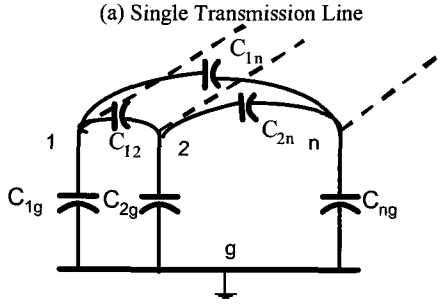

(b) Capacitive elements of n Transmission lines

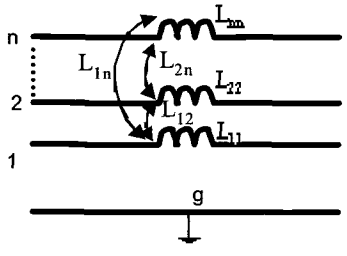

(c) Inductive elements of n Transmission lines

FIGURE 2.3. Equivalent circuit for incremental length of transmission line

a single line are easily extended to multiple lines where V and I are vectors given by

$$V = \begin{bmatrix} V_1 \\ V_2 \\ \vdots \\ V_n \end{bmatrix} \qquad I = \begin{bmatrix} I_1 \\ I_2 \\ \vdots \\ I_n \end{bmatrix}$$

The corresponding capacitances and inductances are multi-dimensional matrices given by

$$[L] = \begin{bmatrix} L_{11} & L_{12} & \cdots & L_{1n} \\ L_{21} & L_{22} & \cdots & L_{2n} \\ \vdots & \vdots & \vdots & \vdots \\ L_{n1} & L_{n2} & \cdots & L_{nn} \end{bmatrix} \qquad [C] = \begin{bmatrix} C_{11} & -C_{12} & \cdots & -C_{1n} \\ -C_{21} & C_{22} & \cdots & -C_{2n} \\ \vdots & \vdots & \vdots & \vdots \\ -C_{n1} & -C_{n2} & \cdots & C_{nn} \end{bmatrix}$$

where $C_{ij} = C_{ji}$ is the mutual capacitance between lines j and i. $C_{ii} = C_{ig} + \Sigma^{n}{}_{j=1,j\neq i} C_{ij}$ is the self-capacitance for the line i, and C_{ig} is the capacitance between line i and ground. Furthermore, L_{ii} is the self-inductance per unit length for the i_{th} line, and $L_{ij} = L_{ji}$ is the mutual inductance per unit length between the i_{th} and j_{th} line.

Equations(2.6) and (2.7) are extended to matrix form

$$\frac{\partial \mathbf{V}}{\partial z} = -[L]\frac{\partial \mathbf{I}}{\partial t} \tag{2.8}$$

$$\frac{\partial \mathbf{I}}{\partial z} = -[C]\frac{\partial \mathbf{V}}{\partial t} \tag{2.9}$$

The $[L]$ and $[C]$ matrices are symmetric. While the elements of the [L] matrix are positive, $[C]$ matrix has positive diagonal terms and negative off-diagonal terms. Also, the sum of each row or column is non-negative.

Assuming the system to be uniform and modal wave propagation with propagation constant β along the z direction of propagation and harmonic time variation, the phase change is of the form $e^{j(\omega t - \beta z)}$. Using phasors to represent voltages and currents, the above equations are re-written as

$$-j\beta V = -j\omega\,[L]\,I \tag{2.10}$$

$$-j\beta I = -j\omega\,[C]\,V \tag{2.11}$$

Eliminating either I or V, the system of equations may be decoupled to give the following relations

$$\beta^2 V = \omega^2 [L][C] V \tag{2.12}$$

$$\beta^2 I = \omega^2 [C][L] I \tag{2.13}$$

These equations can be expressed as

$$([L][C] - \lambda U)V = 0 \tag{2.14}$$

and

$$([C][L] - \lambda U)I = 0 \tag{2.15}$$

with eigenvalue λ

$$\lambda = \frac{\beta^2}{\omega^2}$$

and where U is the identity matrix. The solution to equations (2.14) and (2.15) is an eigenmode problem. The equations suggest that the voltage and current normal modes and propagation constant β can be obtained in terms of the $[L]$ and $[C]$ matrices of the multi-conductor system.

Assuming TEM mode of propagation, Maxwell's equation for the system relating the electric and magnetic field vectors are given by

$$\nabla \times \mathbf{E}_t = -j\omega\mu\mathbf{H}_t \tag{2.16}$$

$$\nabla \times \mathbf{H}_t = -j\omega\epsilon\mathbf{E}_t \tag{2.17}$$

where $\mathbf{E}_t$ is the transverse electric field vector, $\mathbf{H}_t$ is the transverse magnetic field vector, ϵ is the permittivity of the medium and μ is the permeability of the medium. The subscript t corresponds to the transverse components of the vectors. Since the fields are purely transverse, equations (2.16) and (2.17) reduce to the following equations:

$$\mathbf{a}_z \times \frac{\partial \mathbf{E}_t}{\partial z} = -j\omega\mu\mathbf{H}_t \tag{2.18}$$

$$\mathbf{a}_z \times \frac{\partial \mathbf{H}_t}{\partial z} = -j\omega\epsilon\mathbf{E}_t \tag{2.19}$$

$$\nabla_t \times \mathbf{E}_t = 0 \tag{2.20}$$

$$\nabla_t \times \mathbf{H}_t = 0 \tag{2.21}$$

Decoupling of these equations leads to

$$\frac{\partial^2 \mathbf{E}_t}{\partial z^2} + \beta^2 \mathbf{E}_t = 0 \tag{2.22}$$

with propagation constant $\beta = \omega\sqrt{\mu\epsilon}$. A similar equation can be obtained for the transverse magnetic field as

$$\frac{\partial^2 \mathbf{H}_t}{\partial z^2} + \beta^2 \mathbf{H}_t = 0 \tag{2.23}$$

The above equations show that the TEM waves propagate along the lines with a phase velocity of $1/\sqrt{\mu\epsilon}$, which is equal to the velocity of light in that medium. It is known from [29] that if there are $N+1$ conductors, there exist N basic TEM modes of propagation. That is, for N pure-TEM transmission lines, there are N TEM modes, which have the same propagation constants.

The distributed inductance and capacitance matrices of a transmission line system are related to each other for a homogenous air medium by

$$[L_o] = \mu_o\epsilon_o[C_o]^{-1} \tag{2.24}$$

and

$$[C_o] = \mu_o\epsilon_o[L_o]^{-1} \tag{2.25}$$

where the subscript o stands for air or free space. Also

$$[L_o]\,[C_o] = [C_o]\,[L_o]$$

for a homogenous medium. The product is also symmetric and the eigenmodes are orthogonal [29]. This is not true for the propagation modes of multi-lines in an inhomogeneous medium. For inhomogeneous media, $[L][C] \neq [C][L]$ and the product is not symmetric. The eigenmodes are not orthogonal and the eigenvalues may not be real. However, it has been mentioned that the voltage and current eigenmodes have the same eigenvalues, and therefore, the same phase velocities.

The inductance matrix is independent of changes in the dielectric assuming that the magnetic properties remain constant. The eigenvalue equations for voltage and current are re-written in the following equations

$$[L] = \mu_o \epsilon_o [C_o]^{-1} \tag{2.26}$$

$$[C_o] = \mu_o \epsilon_o [L]^{-1} \tag{2.27}$$

The eigenvalue equation for V becomes

$$[C]\,V = \frac{\beta^2}{k_o^2}\,[C_o]\,V \tag{2.28}$$

where

$$k_o^2 = \omega^2 \mu_o \epsilon_o$$

$[C_o]$ is the capacitance matrix for a homogenous air medium and $[C]$ is the capacitance matrix for the inhomogeneous media.

This generalized eigenvalue problem for equation (2.28) can be solved algebraically for a small number of multiple lines. For a large number of lines, numerical techniques are employed to obtain distinctive eigenvalues and eigenmodes. The effective dielectric constant for the modes in inhomogeneous media is defined here as

$$[C]\,V = \epsilon_{eff}\,[C_o]\,V \tag{2.29}$$

where

$$\beta^2 = \omega^2 \mu_o \epsilon_{eff} \epsilon_o \tag{2.30}$$

Once the effective dielectric constant is known, the phase velocity v_{ph} of any mode is calculated by

$$v_{ph} = \frac{c_o}{\sqrt{\epsilon_{eff}}} \tag{2.31}$$

where v_{ph} is the phase velocity of a mode in the actual structure and c_o is the velocity in air or free space. The current normal modes are related to the voltage normal modes by

$$I = v_{ph}\,[C]\,V \tag{2.32}$$

The characteristic line impedance for each mode can be defined as the ratio of line voltage to the current on the same line

$$Z_j^i = \frac{\mathbf{V}_j^i}{I_j^i} \tag{2.33}$$

where the subscript denotes the line and the superscript, the eigenmode. Here, Z_j^i corresponds to the characteristic impedance of the j_{th} line for the i_{th} eigenmode. Using (2.32), it can be re-written as

$$Z_j^i = \frac{V_j^i}{I_j^i} = \frac{1}{v_{ph}^i}\left[\frac{V_j^i}{\Sigma_{k=1}^n C_{jk} V_k^i}\right] \tag{2.34}$$

where C_{ii} is the self-capacitance and $C_{ij} = -C_{ji}$ for $i \neq j$, is the mutual capacitance. The characteristic admittance is correspondingly given by

$$Y_j^i = \frac{I_j^i}{V_j^i} = v_{ph}^i \left[\frac{\Sigma_{k=1}^n C_{jk} V_k^i}{V_j^i}\right] \tag{2.35}$$

It can be summarized from these definitions, that the line parameters are easily computable once the normal values for voltage and current are known. The voltage and current normal modes are in turn dependent on the capacitances and inductances of the system. The analysis of multi-conductor systems should therefore begin with the computation of capacitances and inductances from the field problem. For the sake of simplified illustration, the defining equations for a single line can be derived from the above equations for

$$i = j = n = 1$$

$$CV = \epsilon_{eff} C_o V \tag{2.36}$$

$$\epsilon_{eff} = \frac{C}{C_o} \tag{2.37}$$

$$Z = \frac{1}{v_{ph} C} \tag{2.38}$$

2.2.2. Modal Analysis of CPW transmission lines

There are two fundamental modes of propagation in coplanar transmission lines. This is consistent with the discussions in the previous section as the CPW is a 3-conductor transmission line. The electric field configuration for the even and odd modes is illustrated in Fig. 2.4. The even mode, also known as the CPW mode, has a field that is symmetric about a plane passing through the midpoint of the cross-section, and parallel to the direction of propagation. The odd mode, also referred to as slot-line mode has an anti-symmetric field configuration. There may also exist other modes including surface-modes, which are essentially non-TEM. They are excited in certain structures subject to specific boundary conditions [37], but can be considered non-existent or negligible in most cases.

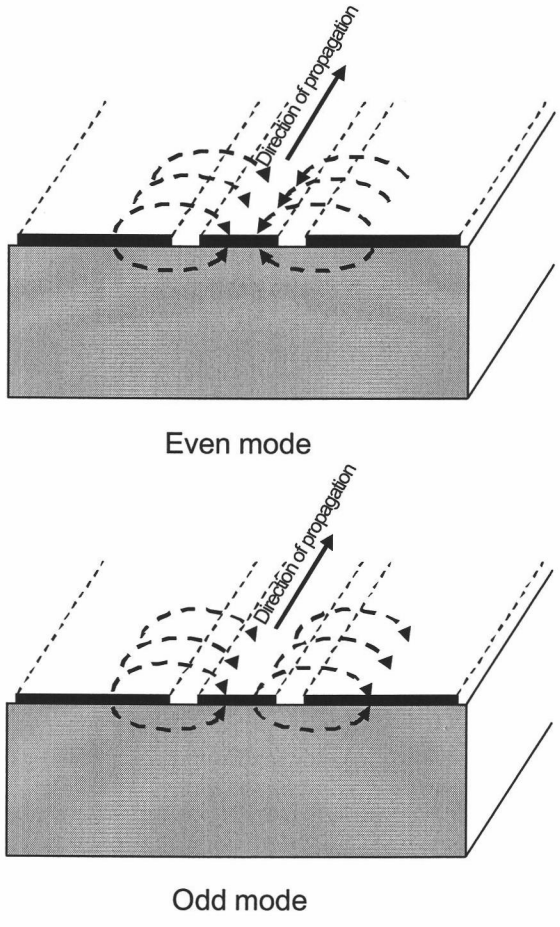

FIGURE 2.4. Modal Field Configuration

In many practical applications, the coplanar structures may be conductor-backed (CB-CPW), *i.e.* a metallization exists on the substrate backside. It is also formed by the chuck of a wafer probe station or the bottom of package. In some cases, it is advantageous to have a bottom metallization plane, as it aids in efficient heat removal. This conductor-backed geometry may cause strange effects, since an additional fundamental mode called the parallel-plate line (PPL) mode or the microstrip (MS) mode appears. Figure 2.5 shows the electric field lines for the PPL mode. The PPL mode is excited due to the voltage difference between the ground

conductors on top of the substrate and backside, and has the same symmetry as the even mode. The CB-CPW comprises four conductors and hence, three fundamental modes of propagation exist. The analysis of the CB-CPW is not a part of this thesis and is not considered.

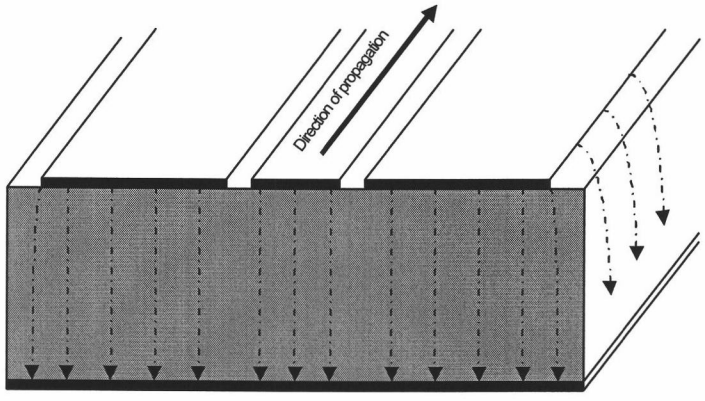

FIGURE 2.5. Parallel-plate mode in a CB-CPW

The solution of the electrostatic or magnetostatic field problem for a given geometrical configuration of conductors and dielectrics characterizes multi-conductor problems. In other words, the modal parameters for a CPW can be found from the capacitance or inductance matrix for the system. The capacitances can easily be extracted from capacitance solvers that use quasistatic 2D methods like quasistatic SDA. The voltages and charges on the conductors are related by the following

$$[Q] = [C]\,[V] \tag{2.39}$$

For a CPW structure, $[C]$ is a 3×3 matrix, and for the sake of discussion, let the three conductors of the CPW be labeled $1, 2$ and 3, respectively, as illustrated

in Fig. 2.6. Equation (2.39) can then be re-written for a three conductor case as follows:

$$\begin{bmatrix} Q_1 \\ Q_2 \\ Q_3 \end{bmatrix} = \begin{bmatrix} C_{11} & -C_{12} & -C_{13} \\ -C_{21} & C_{22} & -C_{23} \\ -C_{31} & -C_{32} & C_{33} \end{bmatrix} \begin{bmatrix} V_1 \\ V_2 \\ V_3 \end{bmatrix} \tag{2.40}$$

where C_{ij} is the capacitance between lines i and j, and

$$C_{ii} = C_{ig} + \Sigma_{j=1,j\neq i}^{3} C_{ij} \tag{2.41}$$

is the self capacitance of line i. Setting C_{ig}=0 due to the ground at infinity, and using (2.41) in (2.40), we have

$$\begin{bmatrix} Q_1 \\ Q_2 \\ Q_3 \end{bmatrix} = \begin{bmatrix} C_{12}+C_{13} & -C_{12} & -C_{13} \\ -C_{21} & C_{12}+C_{23} & -C_{23} \\ -C_{31} & -C_{32} & C_{31}+C_{32} \end{bmatrix} \begin{bmatrix} V_1 \\ V_2 \\ V_3 \end{bmatrix} \tag{2.42}$$

The above equations show that for any given set of applied potentials, the charges induced on any conductor can be determined, once the capacitance matrix is known. Conversely, the capacitance can be determined by finding the induced charges on any conductor for applied potentials on all the conductors. For a general $N+1$ line system, there are $\frac{1}{2}(N+1)N$ independent capacitances because of the symmetry of the $[C]$ matrix. For the CPW under consideration, the capacitances that define the system are C_{12}, C_{13} and C_{23}. The even- and odd- mode capacitances for the CPW can then be determined by forcing the corresponding voltage configurations for the conductors. With the usual assumption that one of the conductors is ground, a reduced 2×2 matrix is obtained.

The reduction of the capacitance matrix to the corresponding even- and odd-mode capacitances is illustrated in Fig. 2.6. To simplify the analysis, the center conductor is fixed to 0V potential *i.e.* ground. The even mode has a symmetric field about the center conductor 2, and therefore, the voltages on conductors 1 and 3

are equal. On the other hand, for the odd mode, which has an anti-symmetric field configuration about the center conductor, the voltages on conductors 1 and 3 are equal in magnitude but opposite in polarity.

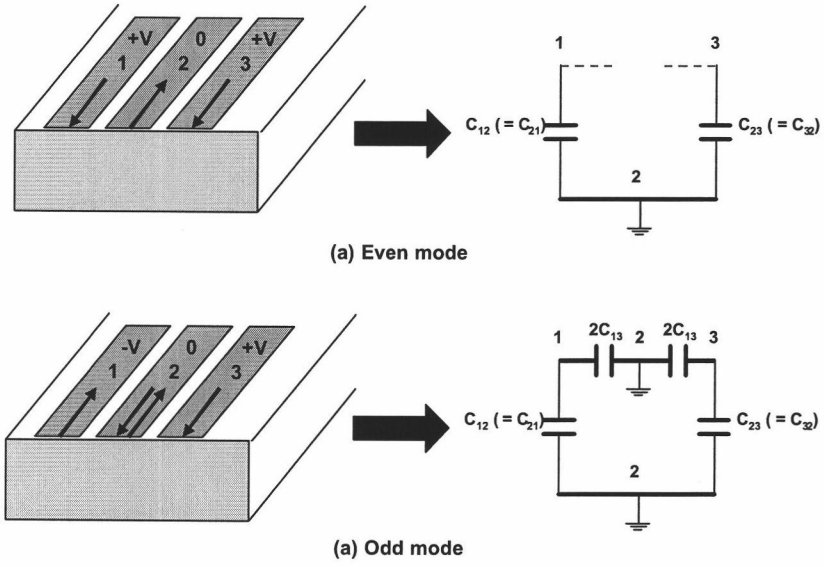

FIGURE 2.6. Even and odd mode excitations and the resulting equivalent capacitance networks

Assuming a symmetric cross-section, the even- and odd- mode capacitances are as given below

$$C_{even} = C_{12} + C_{23} \tag{2.43}$$

$$C_{odd} = C_{12} + 2C_{13} = C_{23} + 2C_{13} \tag{2.44}$$

The procedure for finding the propagation constants and characteristic impedance of the two modes is as follows. A capacitance solver is used twice, once with air dielectric and then with the substrate included. The air and substrate

capacitance matrices can then be reduced to obtain the respective even- and odd-mode capacitances. The effective dielectric constants and characteristic impedances are given by the following equations

$$\epsilon_{even(odd)} = \frac{C_{even(odd)}}{Cair_{even(odd)}} \tag{2.45}$$

$$Z_{even(odd)} = \frac{1}{c}\sqrt{\frac{1}{C_{even(odd)}Cair_{even(odd)}}} \tag{2.46}$$

where c is the velocity in free space equal to 3×10^8m/s. C_{even} is the even mode capacitance for the CPW with the substrate included and $Cair_{even}$ is the even-mode capacitance of the structure in a homogeneous air dielectric. A similar definition is applied to the odd mode.

2.3. Discontinuities in Coplanar Waveguide

Microwave networks often consist of transmission lines with various types of discontinuities. In most cases discontinuities are an unavoidable result of mechanical or electrical transitions from one medium to the other. The discontinuity is usually unwanted but may be significant enough to warrant characterization. In other cases, the discontinuities may be deliberately introduced in the circuit to perform a certain electrical function. Examples include directional couplers, power dividers and filter circuits. In any event, a discontinuity in the transmission line needs to be represented by an equivalent circuit for analysis purposes. Depending on the type of discontinuity, the equivalent circuit may be a simple shunt or series element, or more complex comprising many elements. The component values of an equivalent circuit depend on the parameters of the line, discontinuity, and the frequency of operation. In some cases, the equivalent circuit requires a shift in the phase reference planes of

the transmission lines [39]. Discontinuities in CPW transmission lines is the subject of discussion in this section.

Examples of common discontinuities in CPWs were shown in Fig. 1.2. As discussed in the previous section, the CPW supports more than one fundamental mode of transmission. The study of discontinuities is therefore a multi-modal problem, where the interaction between the modes is important. Discontinuities in a CPW have been treated and analyzed in the past as four-port model [4], [5] - [8]. The coupling between modes is characterized by a 4x4 modal scattering matrix. Figure 2.7 illustrates a general four-port description for a CPW discontinuity. The subscripts e and o refer to the even- and odd- modes, respectively. It is assumed in Fig. 2.7 that only these two fundamental modes in the CPW feed lines exist. The model therefore consists of two ports for each of the modes, one on each side of the discontinuity. The two even-mode ports are 1 and 2, while ports 3 and 4 correspond to the odd mode on either side of the discontinuity.

There are other discontinuities like the CPW-to-microstrip transition or CB-CPW discontinuities that excite the PPL mode on one side of the discontinuity. In this case, the network in the figure has to be correspondingly modified to a 5-port or 6-port model. It is seen that the analysis can become increasingly complex for structures with more than two modes.

In general, the description of the discontinuity in terms of the modal matrices is very convenient for analysis purposes. The modal description of a discontinuity contains sufficient information to characterize it completely. Modal analysis has been performed on several CPW discontinuities in the past. Full-wave EM techniques have been applied to directly extract the modal scattering parameters at the discontinuities [4], [5], [23]. In [4], a CPW right-angle bend is characterized using mixed-potential integral formulation, and a four-port model for the disconti-

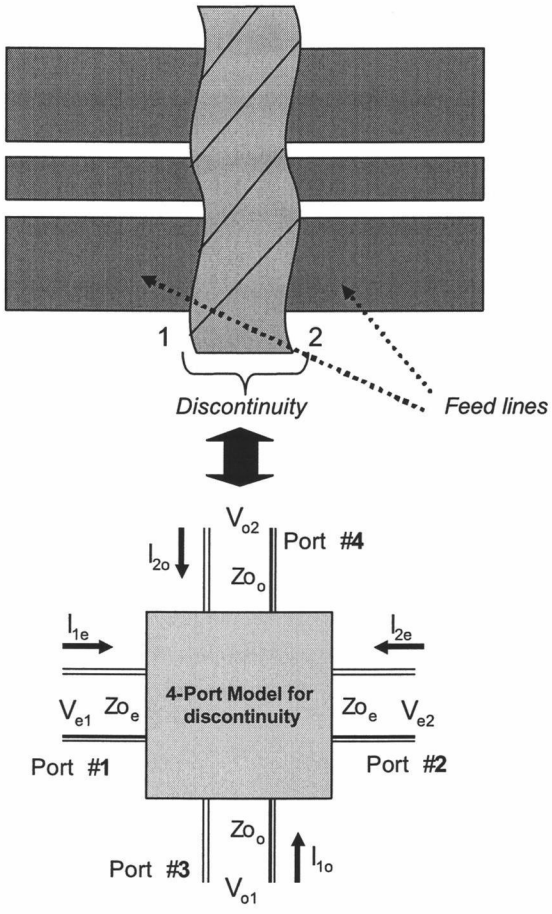

FIGURE 2.7. Generalized four-port model for CPW discontinuity

nuity has been proposed. The four-port modal scattering matrix includes the effect of coupling between the modes and mode conversion. CPW-to-slot line transitions have been analyzed in [23]. Reference [8] performs the modal analysis of shunt stubs in CPW using a space-domain integral equation (SDIE).

Examples of symmetric and asymmetric discontinuities are given in Fig. 2.8. The asymmetric discontinuities, by virtue of their geometry, excite the odd mode. This phenomenon of mode conversion is significant and requires accurate characterization, as it involves loss of power from the desired mode of operation. Several

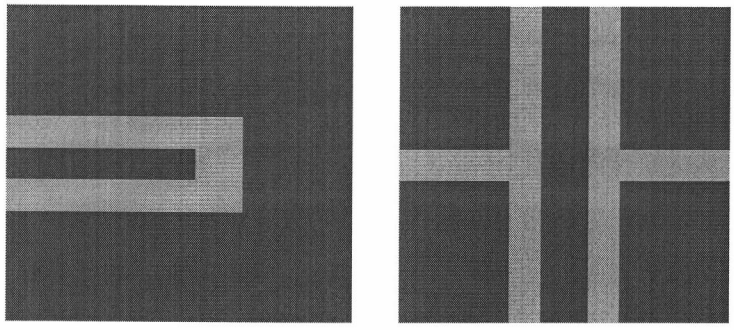

Open stub *Two-sided shunt stub*

(a) Symmetric discontinuities

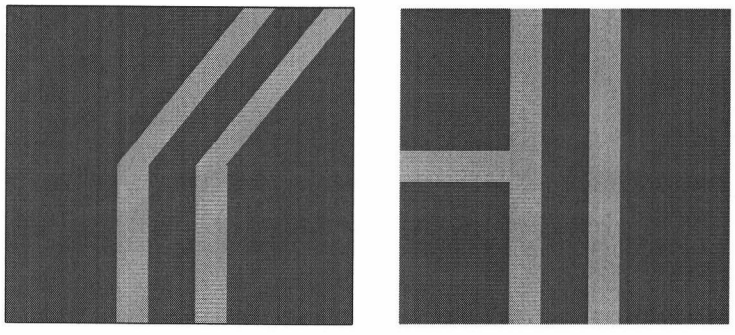

Bend *Asymmetric shunt stubs*

(a) Asymmetric discontinuities

FIGURE 2.8. CPW Discontinuities

methods have been proposed to suppress the odd mode at discontinuities including the use of air bridges [7] or top or bottom ground plane shields [11]. Physically tying together the two outer conductors of a CPW tends to suppress the asymmetric odd mode. Mitering has also been used to compensate the bend such that it minimizes the mode conversion. The following chapter seeks to develop a four-port model for the CPW bend to accurately characterize mode conversion.

2.4. Conclusions

The solution of the electrostatic field problem for a given geometrical configuration of conductors and dielectrics leads to the characterization of multi- conductor problems. The CPW is a two-mode structure, and the modal properties can be obtained from the distributed capacitances of the three-conductor system. Therefore, discontinuities in the CPW need to be characterized by a two-mode (four-port) network model. Asymmetric discontinuities like bends and one-sided shunt stubs excite a parasitic odd mode through mode conversion. The next chapter deals with developing four-port models to characterize this mode conversion in CPW bends.

3. MODELING OF COPLANAR WAVEGUIDE BENDS

3.1. Introduction

Bends are among the most common interconnect discontinuities. They have become an integral part in present-day ICs and PCBs due to the complex routing of signal paths that exists. A bend in the CPW generates an unwanted odd mode by virtue of its asymmetry. This excitation of the parasitic mode can create problems with the normal operation of CPW circuits. A thorough and rigorous approach to study the effects of the bend is therefore needed. Models for the bend discontinuity that characterize it completely would greatly help in the design of CPW-based RF circuits.

This chapter starts with a review of coupled transmission line theory. The voltage-current relationships for coupled transmission lines, which includes the contributions due to the mutual capacitances and inductances, are derived. These relationships are later applied in the analysis of CPWs. A CPW can be considered as two coupled quasi-slot transmission lines running parallel to each other. A bend in the CPW is therefore a non-uniform coupled line system. The analysis of coupling effects around the bend is then discussed, and a quasistatic model for the bend section is developed. The model has four ports corresponding to the four slots in the bend. Relations between the slot voltages and the modal voltages are then used to obtain a four-port modal scattering matrix. The modal scattering matrix contains information regarding the transmission coefficients between the modes and the modal reflection coefficients.

As explained later in this chapter, this modal information proves useful in the study of mode at discontinuities. Modal transmission coefficients derived from

the model have been compared with the results obtained from full-wave simulations. The comparisons are shown for structures with different dimensions to demonstrate the applicability of the model to a wide variety of geometries. The effect of the center conductor width, slot spacing, and dielectric permittivity on mode conversion and resonances in the structure are also discussed in detail.

3.2. Theory of Coupled Transmission Lines

Transmission lines consist of multiple parallel conductors that are in close proximity to each other. One of the most common examples is that of parallel-running signal lines on PCBs. Due to the close proximity of the conductors, the time-varying electric and magnetic fields generated by different lines interact, giving rise to electromagnetic coupling between the transmission lines. As a result, the voltage-current relationships for these lines include the effects of electric and magnetic field coupling that exists between the lines. Coupling between adjacent transmission lines is often unwanted and deteriorates the performance of the system. There is loss of power from the signal line to the adjacent lines through coupling, which can induce crosstalk and other compatibility problems. In other applications, the coupling between transmission lines is used to achieve certain functionalities such as power-division, filtering, etc. The following sections review the analysis of a pair of coupled transmission lines.

Unlike circuit theory, transmission line theory deals with the analysis of transmission lines with length comparable to the wavelength. This calls for a distributed-parameter network, where voltages and currents can vary in magnitude and phase over its length. Figure 3.1(a) shows a short section of a transmission line of length dz. This incremental line section can be modeled as a lumped element circuit, as shown in Fig. 3.1, where R, L, G, C are per-unit length quantities defined as follows

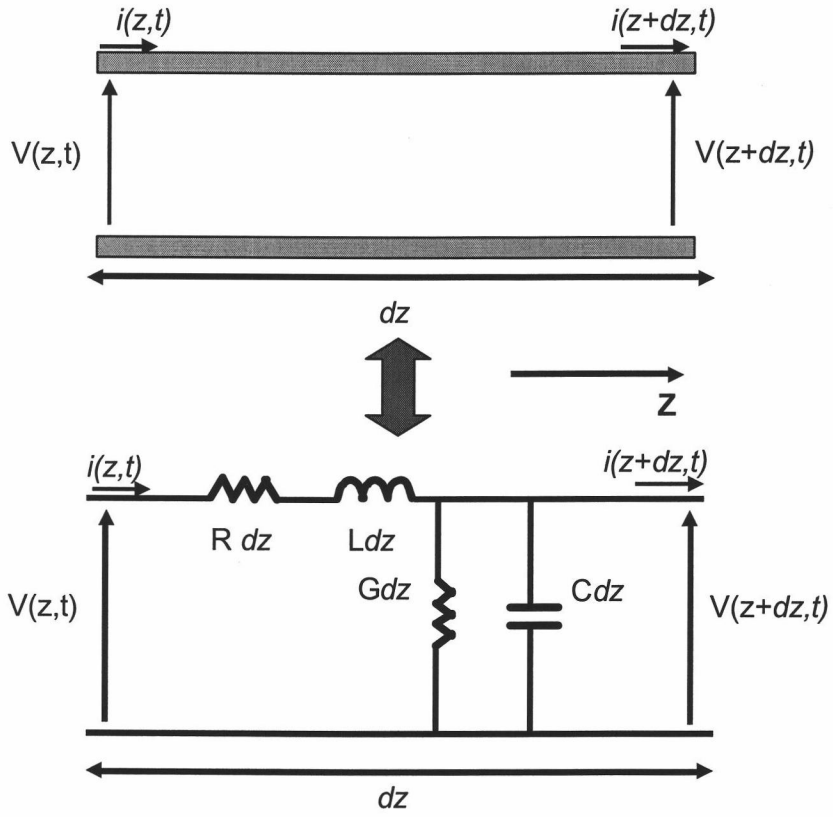

FIGURE 3.1. Lumped-element equivalent circuit for incremental length of transmission line

R = series resistance per unit length, in Ω/m

L = series inductance per unit length, in H/m

G = shunt conductance per unit length, in S/m

C = series capacitance per unit length, in F/m

The following equations for voltage and current can be derived

$$\frac{\partial v(z,t)}{\partial z} = -Ri(z,t) - L\frac{\partial i(z,t)}{\partial t} \tag{3.1}$$

$$\frac{\partial v(z,t)}{\partial z} = -Gi(z,t) - C\frac{\partial v(z,t)}{\partial t} \tag{3.2}$$

Assuming $v(i,t)$ and $i(z,t)$ are cosine-based phasors, the equations reduce to

$$\frac{dV(z)}{dz} = -(R + j\omega L)I(z) \tag{3.3}$$

$$\frac{dI(z)}{dz} = -(G + j\omega C)V(z) \tag{3.4}$$

The above set of partial differential equations can be extended to describe the interdependence between the line voltages and currents in a two coupled-line system. Figure 3.2. shows the equivalent circuit for an incremental length of two-coupled transmission lines. The distributed capacitance between line 1 and the ground conductor labeled g is C_{1g}, and the distributed capacitance between line 2 and ground is C_{2g}. The distributed mutual capacitance between the two lines is C_m. Similarly, L_1 and L_2 are the distributed inductances associated with the two lines 1 and 2 repectively, while L_m is the distributed mutual inductance between the two transmission lines. The distributed resistances $R_{1,2}$ and conductances $G_{1,2}$ can be defined accordingly.

The interdependence relations for the line voltages and currents are obtained by considering the change in electric and magnetic flux linkage as a function of time for an incremental section of the line. The resulting set of partial differential equations for voltages and currents on the lines is given by

$$\begin{bmatrix} \frac{\partial I_1(z,t)}{\partial z} \\ \frac{\partial I_2(z,t)}{\partial z} \end{bmatrix} = -\begin{bmatrix} G_{11} & G_{12} \\ G_{21} & G_{22} \end{bmatrix} \begin{bmatrix} V_1(z,t) \\ V_2(z,t) \end{bmatrix} - \begin{bmatrix} C_{11} & C_{12} \\ C_{21} & C_{22} \end{bmatrix} \begin{bmatrix} \frac{\partial V_1(z,t)}{\partial t} \\ \frac{\partial V_2(z,t)}{\partial t} \end{bmatrix} \tag{3.5}$$

where

$$\begin{bmatrix} C_{11} & C_{12} \\ C_{21} & C_{22} \end{bmatrix} = \begin{bmatrix} C_{1g} + C_m & -C_m \\ -C_m & C_{2g} + C_m \end{bmatrix} \tag{3.6}$$

and

$$\begin{bmatrix} \frac{\partial V_1(z,t)}{\partial z} \\ \frac{\partial V_2(z,t)}{\partial z} \end{bmatrix} = -\begin{bmatrix} R_{11} & R_{12} \\ R_{21} & R_{22} \end{bmatrix} \begin{bmatrix} I_1(z,t) \\ I_2(z,t) \end{bmatrix} - \begin{bmatrix} L_{11} & L_{12} \\ L_{21} & L_{22} \end{bmatrix} \begin{bmatrix} \frac{\partial I_1(z,t)}{\partial t} \\ \frac{\partial I_2(z,t)}{\partial t} \end{bmatrix} \tag{3.7}$$

where

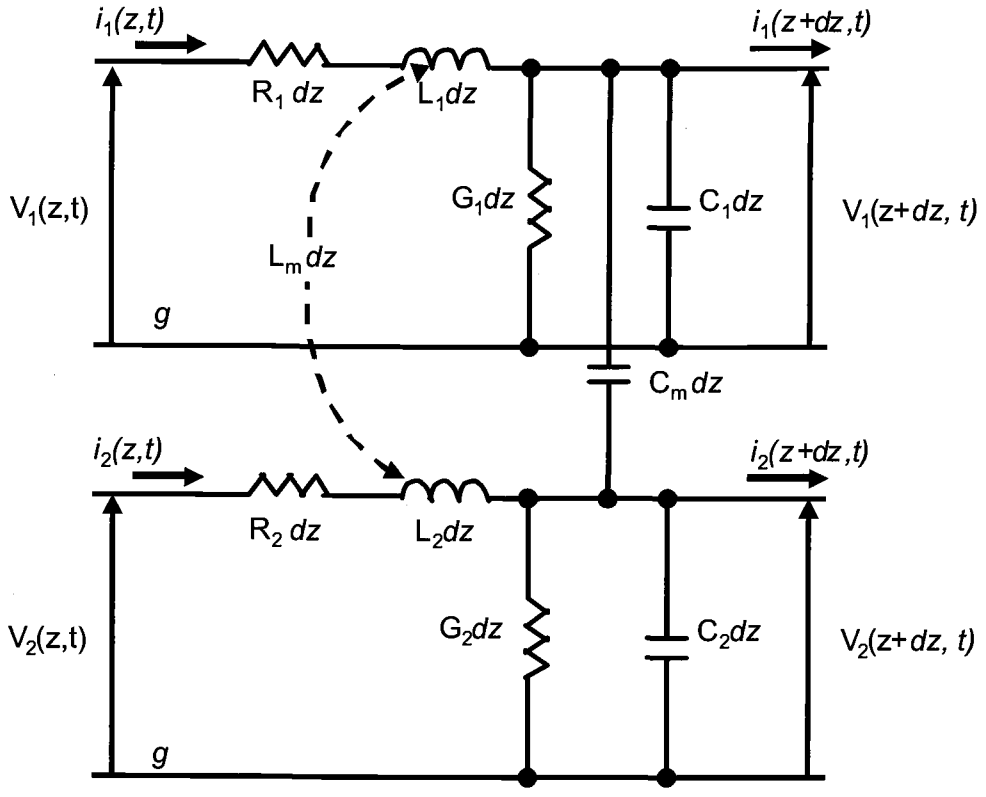

FIGURE 3.2. Lumped-element equivalent circuit for incremental length of two coupled transmission lines

$$\begin{bmatrix} L_{11} & L_{12} \\ L_{21} & L_{22} \end{bmatrix} = \begin{bmatrix} L_1 & L_m \\ L_m & L_2 \end{bmatrix} \tag{3.8}$$

For lossless lines, the series resistance and the shunt conductance terms are zero. Neglecting the resistance and conductance terms, 3.5 and 3.7 reduce to

$$\begin{bmatrix} \frac{\partial I_1(z,t)}{\partial z} \\ \frac{\partial I_2(z,t)}{\partial z} \end{bmatrix} = -\begin{bmatrix} C_{11} & C_{12} \\ C_{21} & C_{22} \end{bmatrix} \begin{bmatrix} \frac{\partial V_1(z,t)}{\partial t} \\ \frac{\partial V_2(z,t)}{\partial t} \end{bmatrix} \tag{3.9}$$

and

$$\begin{bmatrix} \frac{\partial V_1(z,t)}{\partial z} \\ \frac{\partial V_2(z,t)}{\partial z} \end{bmatrix} = -\begin{bmatrix} L_{11} & L_{12} \\ L_{21} & L_{22} \end{bmatrix} \begin{bmatrix} \frac{\partial I_1(z,t)}{\partial t} \\ \frac{\partial I_2(z,t)}{\partial t} \end{bmatrix} \tag{3.10}$$

It can be inferred from the above equations that the voltages and currents on any one line depend on the rate of change of currents and voltages on the other line. This dependence is stronger for higher values of the mutual terms C_{12} and L_{12}, and vice versa. This mathematical description of two coupled transmission lines can be readily extended to any N transmission lines. The corresponding current and voltage vectors are Nx1 and the distributed parameter matrices are NxN.

A general two coupled-line system can be described in terms of a four-port network. The network parameters such as impedance or admittance matrices can be conveniently derived from the frequency-domain even- and odd mode responses of the system. Simple equivalent circuits can in turn be derived from the four-port network parameters. Other network representations that describe a general system include the ABCD matrix and scattering matrix. Knowing any one of these parameters, the other network parameters can be derived to better suit the analysis of a problem at hand.

3.3. CPW as coupled quasi-slot lines

The geometry of a typical slot line is shown in Fig. 3.3 (a). It consists of a slot or gap in an infinite metallic plane on a dielectric substrate. The electric field lines in a slot transmission line lie across the slot. This enables discrete components to be shunt mounted on the slot lines. The characteristic impedance of the slot line depends to a large extent on the slot width. The wider the slot is, the greater the characteristic impedance, and vice versa. Since the mode of propagation along the line is non-TEM, the characteristic impedance shows a strong dependence on the frequency of operation as well. While the metallization is laterally infinite in slot lines, a similar structure with finite metallization as shown in Fig. 3.3 (b) can be considered as a quasi-slot line. Like the slot line, the quasi-slot line supports a

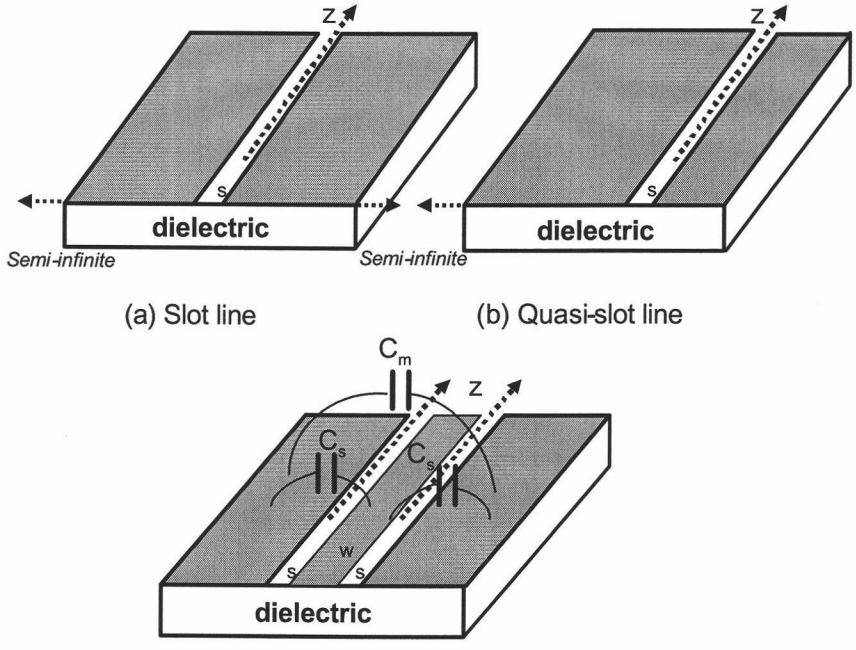

FIGURE 3.3. Slotline and CPW

non-TEM mode of propagation but can be considered as quasi-TEM for analysis purposes at low frequencies.

The CPW can be viewed as a pair of coupled parallel quasi-slot lines. For example, consider the CPW shown in Fig 3.3 (c). The center conductor width is w and the separation between the slots is s. This configuration is equivalent to that of two coupled quasi-slot lines of width s separated by a distance w. The center conductor of the CPW can be assumed to be the common ground for the slot transmission lines. Thus, the capacitance C_m shown in the figure is nothing but the mutual coupling capacitance of the two quasi-slot lines. As discussed in the previous chapter, the capacitance matrix for a multi-conductor system is obtained easily using

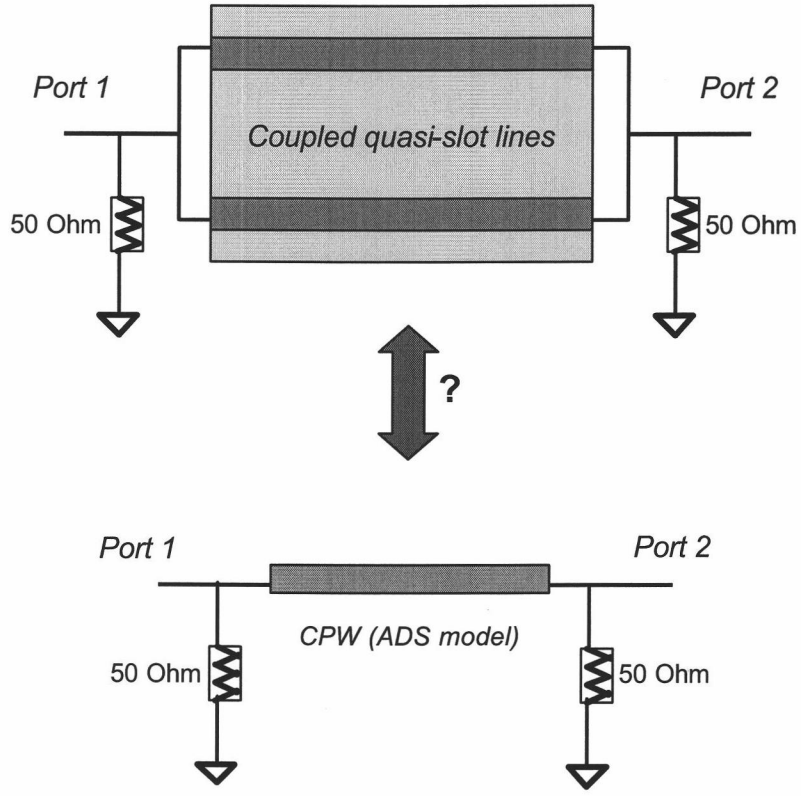

FIGURE 3.4. Circuit Schematics: Parallel coupled quasi-slot lines vs. CPW

2D capacitance solvers. The parameters of the coupled slot lines in Fig. 3.3. are derived from the capacitance matrix of the corresponding three-conductor system.

For sake of comparison, consider the two circuit schematics shown in Fig. 3.4. The first one is that of a coupled quasi-slot line with the lines tied together at both ends. This is the equivalent of a CPW with outer conductors shorted together. The even mode of propagation in a CPW has a symmetric field configuration about the center conductor. Thus, forcing the outer conductors to the same potential, only the even mode exits in the structure. By simulating the shorted coupled lines and comparing the S-parameters with that of a CPW model in the commercially available

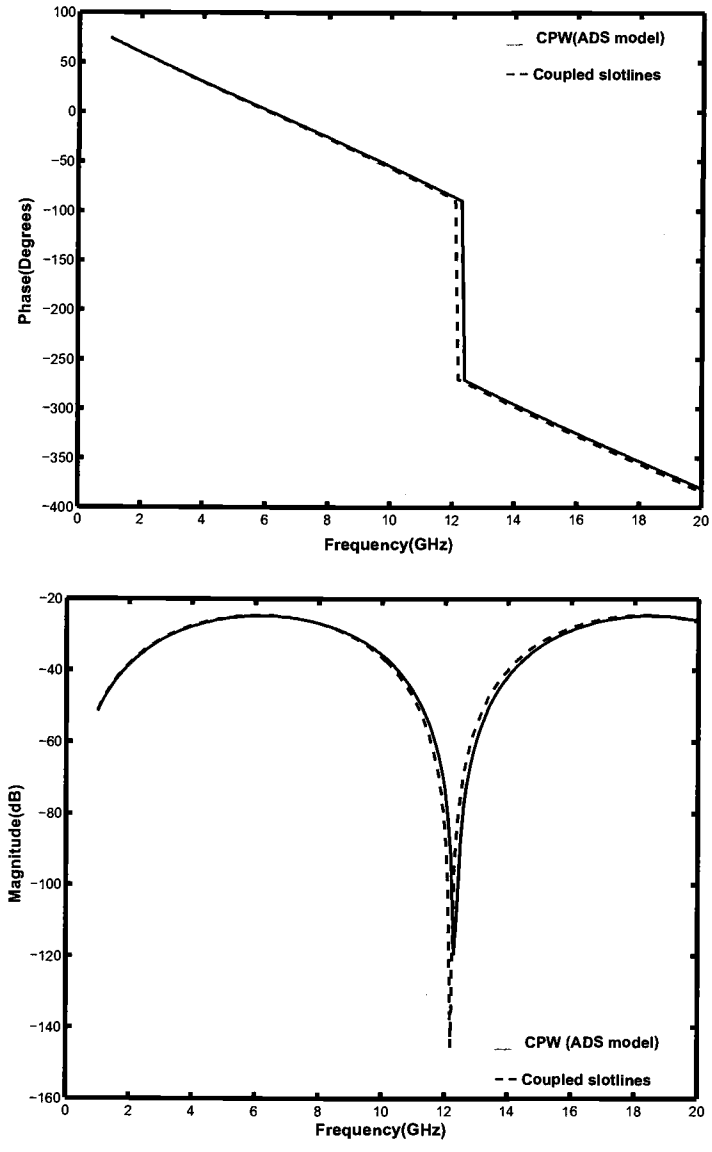

FIGURE 3.5. Comparison of S(1,1)

tool ADS [31], it can be ascertained if the coupled quasi-slot line description of a CPW fits well. Figures 3.5. and 3.6. plot the S-parameters with 50 Ω reference port impedances. A length l of 20mm is chosen with the slot spacing $s = 0.6$mm and the center conductor width $w = 5$mm.

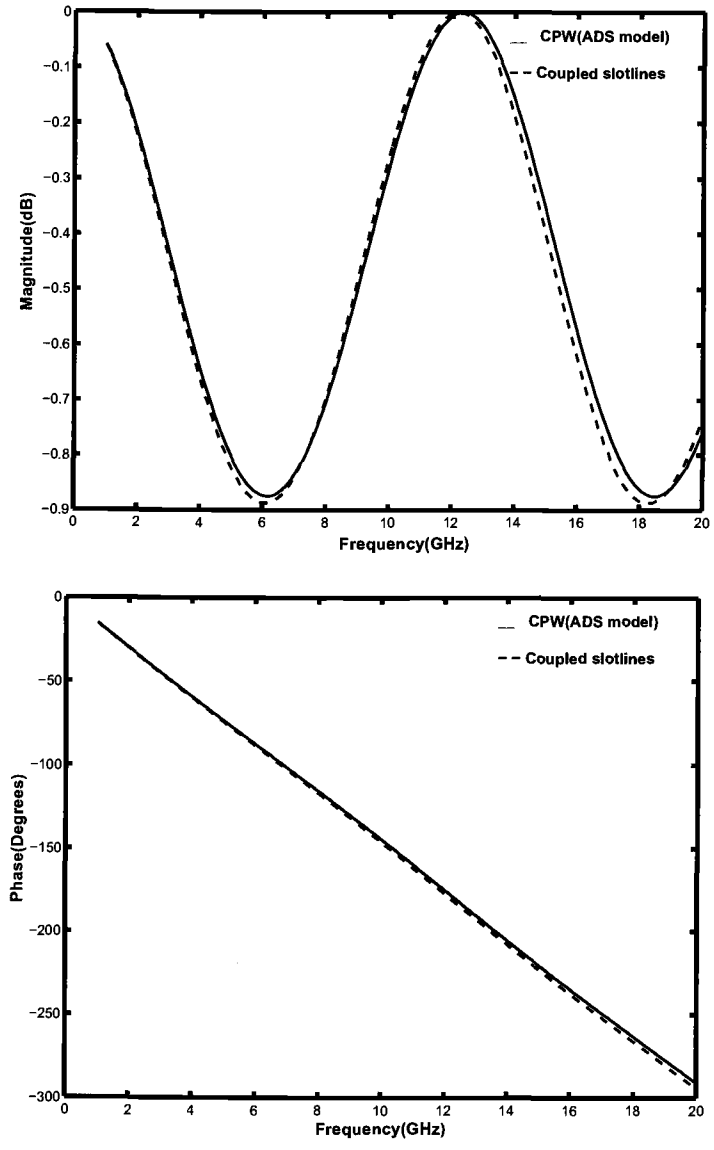

FIGURE 3.6. Comparison of S(1,2)

It is seen from the plots that the quasi-static coupled line description approximates the CPW model well at low frequencies. As the frequency of operation increases, there is a slight mismatch in S-parameters. This may be due to finite-width approximation for the two outer conductors in extracting the 3 x 3 capacitance

matrix. Coupled quasi-slot lines in general can be considered a good approximation of the CPW.

3.4. Model Development

This section gives a detailed explanation of the approach presented in [41] for the modeling of CPW bends. A bend in the coplanar structure is inherently a non-uniform coupled line structure with different line lengths. Figure 3.7 shows a CPW right-angle bend with center conductor b of width w and slot-width s. The two outer conductors are labeled a and c. This non-uniform coupled line system has two predominant effects on signal propagation in the slots around the bend. First of all, it introduces a phase difference between the signals in the slots due to the different lengths around the bend. Secondly, there is tight coupling between the slots that is not uniform along the length of the bend. The signals propagating along the two slots have a continuously changing degree of cross-coupling around the bend geometry. Looking at the bend in Fig. 3.7, as we move from reference plane R1 to reference plane R2, the mutual capacitance per unit length C_{ac} is not a constant and varies continuously. It reduces to the lowest value around the corner of the bend where the separation between the slots is maximum, and then increases back to the initial value. The value of C_{ac} at the reference planes R1 and R2 is equal to the mutual capacitance between the quasi-slot lines feeding the bend.

To analyze the non-uniform coupling that takes place in the bend more closely, consider the two structures shown in Fig. 3.8. Figure 3.8 (a) shows a right-angle CPW bend without the feed lines and Fig. 3.8 (b) is a hypothetical structure obtained by straightening of the bend. The structure in Fig. 3.8 (b) serves as a good starting point in the analysis of non-uniform coupling in the bend.

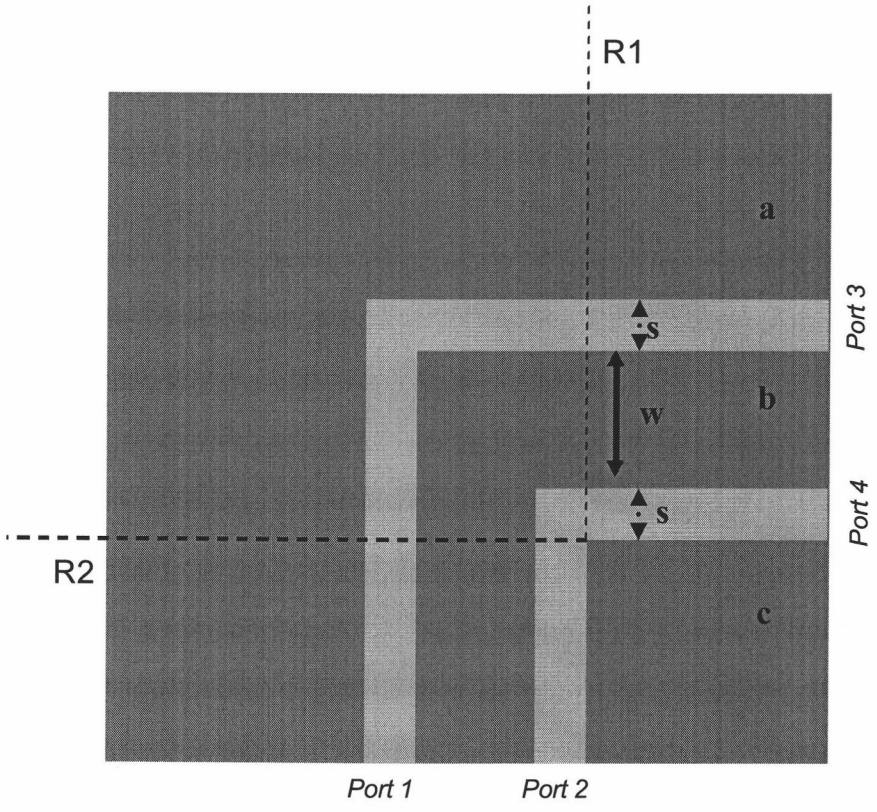

FIGURE 3.7. CPW Right-Angled Bend

It is known that the charge density is higher at the edges of conductors in the bend. The charges in one of the outer conductors of the CPW bend are illustrated in Fig. 3.8. By a first order approximation, the net charge in the two outer conductors of the CPW is assumed to be concentrated at the edges, as line charges. The mutual capacitance per unit length (p.u.l) between two incremental charge elements on these two line charges is equal to C_m. Thus, the capacitance between the elements A and B shown in Figure 3.8 (a) and (b) is C_m.

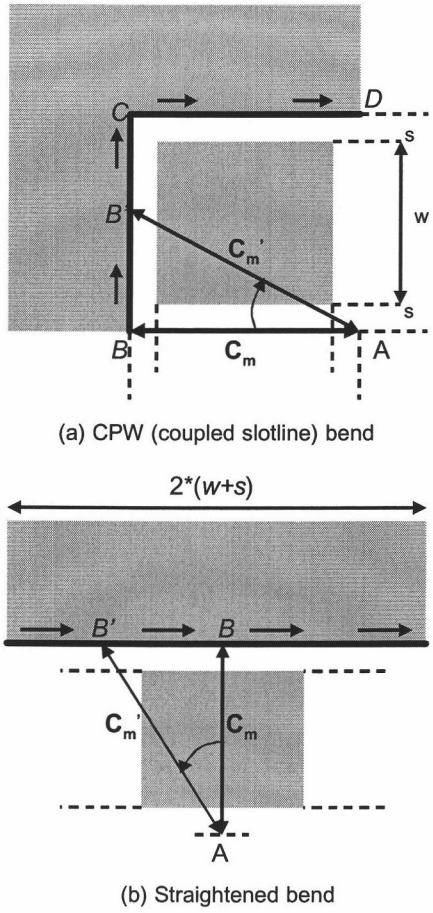

FIGURE 3.8. Illustration of coupled line geometries

The capacitance between any two charge elements is inversely proportional to the separation between the elements. The capacitance between the elements A and B' can therefore be approximately expressed interms of C_m as

$$C_m' = C_m \times \frac{AB}{AB'} \tag{3.11}$$

where

$$AB' = \frac{AB}{\cos(\theta)} \tag{3.12}$$

Using (3.12) in (3.11) gives

$$C_m' = C_m \times \cos(\theta) \tag{3.13}$$

It is seen from equation (3.11) that the mutual capacitance C_m between incremental line charges, which is also interpreted as the p.u.l. capacitance between the two coupled quasi-slot lines, is not constant around the bend. For example in Fig. 3.8 (a), for the signals traveling from one side to the other, the coupling capacitance is the strongest at the begining of the bend equal to C_m. It reduces to a lowest value at the corner of the bend to $C_m/\sqrt{2}$ and then increases back to the initial value of C_m at D. The coupling between the lines in the straightened bend structure in Fig. 3.8 (b) shows a similar behavior.

Considering the straightened bend structure in Fig. 3.8 (b), the total mutual coupling between the incremental element A and the incremental elements on the other conductor is obtained by integrating equation (3.13) over a length $2*(w+s)$.

$$C_{total} = \int_{-(w+s)}^{w+s} C_m \cos(\theta) dr \tag{3.14}$$

where

$$dr = (w + 2*s)\sec(\theta)^2 d\theta \tag{3.15}$$

is obtained by differentiating

$$r = (w + 2*s)\cos(\theta) \tag{3.16}$$

Using (3.15) in (3.14)

$$C_{total} = 2 \times \int_0^{\frac{\pi}{4}} \frac{C_m(w + 2*s)d\theta}{\cos(\theta)} \tag{3.17}$$

The integration gives a total coupling capacitance equal to

$$C_{total} = 2 \times 0.3827(w + 2*s)C_m = 0.765(w + 2*s)C_m \tag{3.18}$$

This value of total capacitance is approximately equal to the net mutual capacitance between two uniform coupled quasi-slot lines with a p.u.l. capacitance C_m, over a length 0.765*$(w + 2 * s)$. Thus, uniform coupled-lines with an equivalent length of

$$l_{eq} = 0.765 * (w + 2 * s) \tag{3.19}$$

and p.u.l. mutual capacitance C_m can be used to model the non-uniform coupled-line system in Fig. 3.8 (b).

Figure 3.9 illustrates the general methodology for modeling a non-uniform coupled line system. The model consists of a uniform coupled-line section of length given by equation (3.19) cascaded with uncoupled transmission line sections. The coupled line section is of length given by equation (3.19), and supplies the required mutual capacitance. The uncoupled transmission line sections introduce the necessary phase-difference between the two slots in the bend. The phase shift introduced by the coupled line section can be cancelled out by adjusting the feed length of feed lines connected to the bend, or approximately by adjusting the lengths of the uncoupled transmission line sections as illustrated in Fig. 3.10.

The parameters for each of the blocks in Fig. 3.10 are obtained using quasistatic 2D methods. 2D solvers use the cross-sectional information to solve for the 3x3 capacitance matrix for the system. The capacitance matrix can then be reduced to get the coupled line parameters, even- and odd mode impedances (Zo_e, Zo_o) and propagation constants (β_e, β_o). The corresponding set of equations that relate the modal impedance and propagation constants to the capacitances of the system were given in Chapter 2.

The right-angle bend in Fig. 3.8 (a), being a non-uniform coupled structure, is modeled using the same approach given above for Fig. 3.8 (b). However, there is one salient point that should be addressed when developing a model for the right-angle bend. The bend couples the two slot lines more tightly compared to a straight

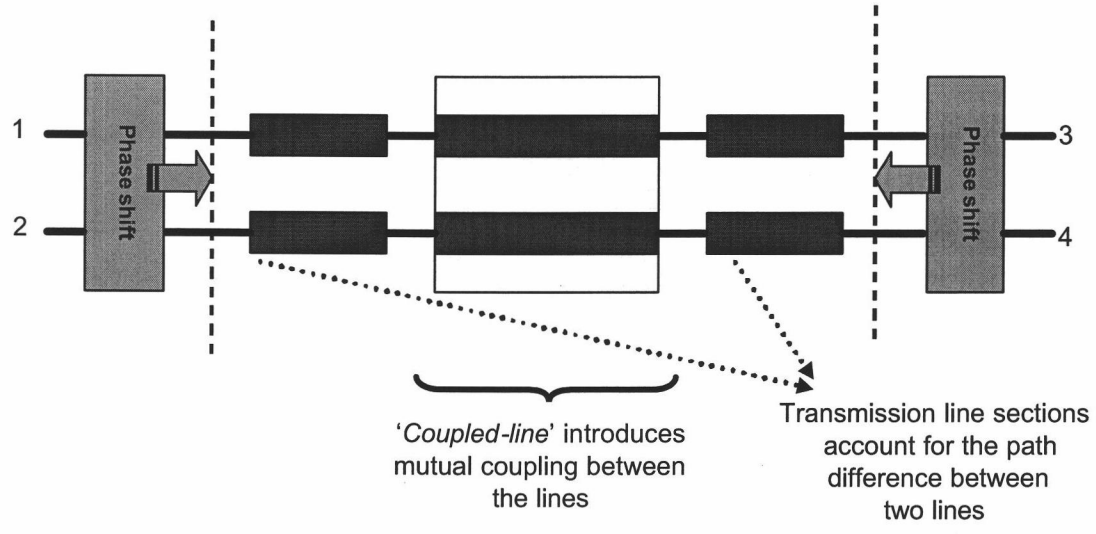

FIGURE 3.9. Approximate modeling of a non-uniform coupled line structure

section. This is because of the closer proximity of the ports at the far-end compared to a straight coupled line. This feature of the bend discontinuity therefore warrants some modifications in the coupled line parameters of the model. It has been found that a factor k can account for the stronger coupling if the even- and odd mode impedances of the coupled-lines are modified as

$$Zo_{ec} = Zo_e * k_e, Zo_{oc} = \frac{Zo_o}{k_o} \tag{3.20}$$

where

$$k = k_e = k_o = 1.6$$

The four-port model for a right-angle CPW bend in shown in Fig. 3.10. It consists of a uniform coupled-line section cascaded with uncoupled transmission line sections. $P1 \cdots P4$ are the four ports of the model, which correspond to slot excitations. The

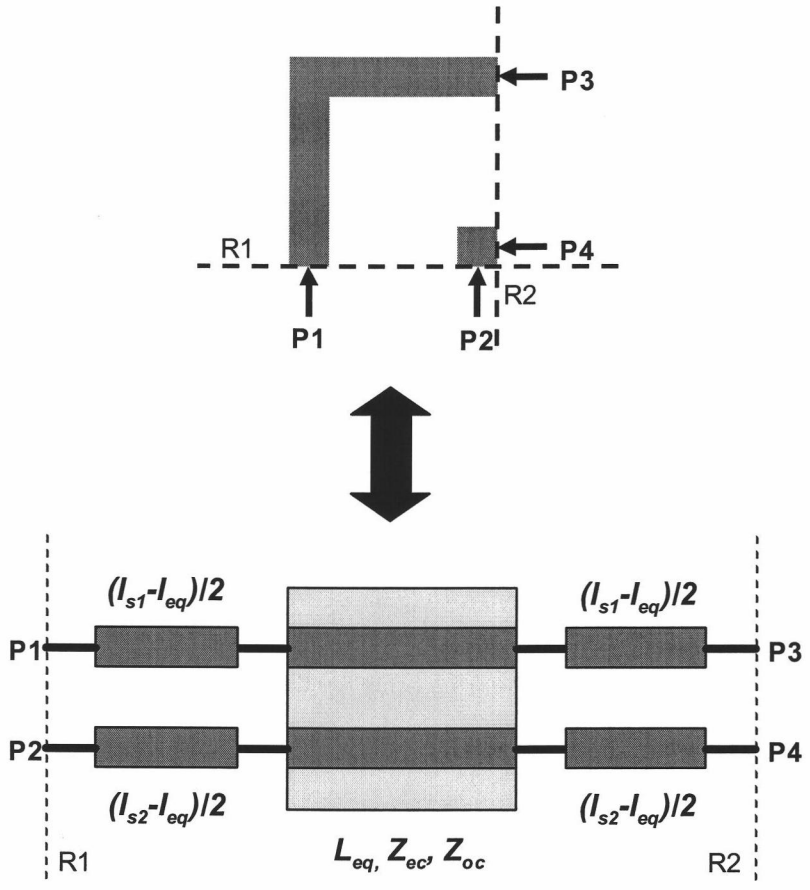

FIGURE 3.10. Model for a CPW right-angle bend

parameters of the coupled line include the effect of stronger coupling in the bend, and the transmission line lengths are adjusted to include the de-embedding effect. The lengths l_{s1} and l_{s2} in the model are the physical lengths of the two slot lines in the bend.

$$l_{s1} = w + 1.5 * s, l_{s2} = 0.5 * s \tag{3.21}$$

The four-port modeling methodology can be easily extended to bends with different angles. In all cases, the model parameters are obtained using the same

approach described above. The model parameters for a 45 degree bend shown in Fig. 3.11. are derived as

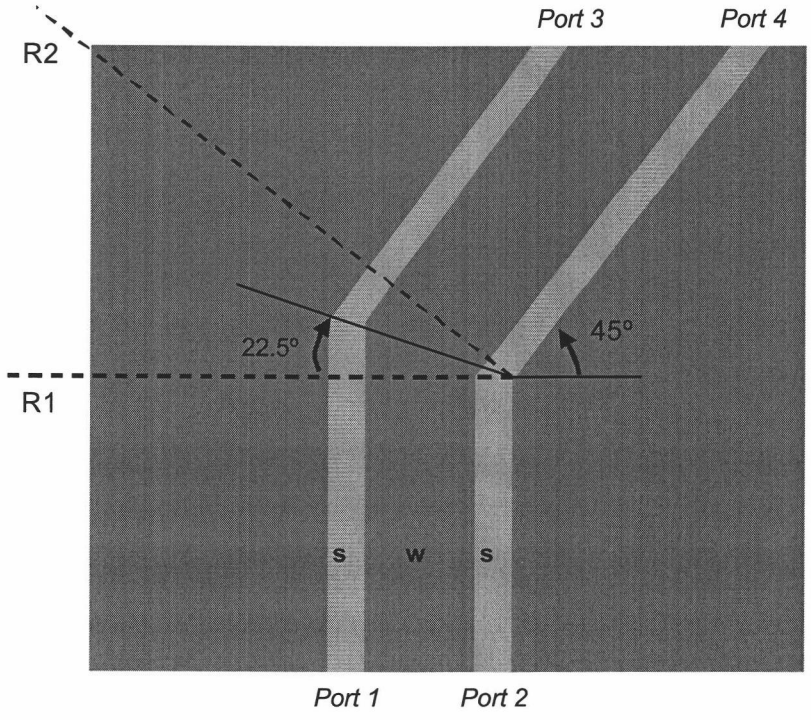

FIGURE 3.11. 45 degree CPW bend

$$\textbf{Coupled-line length:} \quad l_c = 0.35 * (w + 2 * s) \tag{3.22}$$

$$\textbf{Coupled-line impedances:} \quad Zo_{ec} = Zo_e * k_e, Zo_{oc} = \frac{Zo_o}{k_o} \tag{3.23}$$

$$\textbf{Transmission line lengths:} \quad l_{s1} = 0.414 * (w + 1.5 * s), l_{s1} = 0.207 * s \tag{3.24}$$

where k_e and k_o are the even- and odd mode coupling factors. The coupling between the slots is weaker in the 45 degree bend compared to the right-angle case due to the

spreading of fields in the bend region. Unlike the right-angle bends, the coupling factors k_e and k_o are also found to be different for the 45 degree bends. Bends with different dimensions of w and s were studied to estimate the value of these coupling coefficients. A good fit between the model and full-wave simulation results is found for the following values

$$k_e = 1.35, k_o = 1.15 \tag{3.25}$$

It is also seen from equation (3.24) that the path-length difference between the slots is less compared to a right-angled bend. This is obvious by looking at Fig. 3.11.

In summary, the development of a four-port model for the CPW bend was discussed. The model is based on the decomposition of the coplanar waveguide into two coupled quasi-slot lines. The four ports of the model therefore correspond to the four slot excitations, two on each side of the bend. For an arbitrary excitation of the structure, the electric field in each slot is a superposition of the even- and odd mode fields.

3.5. Modal Scattering Matrix

The slot-voltage scattering matrix for the model, which relates the incoming and outgoing waves, is given by

$$\begin{bmatrix} V_1^+ \\ V_2^+ \\ V_3^+ \\ V_4^+ \end{bmatrix} = \begin{bmatrix} S_{11} & S_{12} & S_{13} & S_{14} \\ S_{21} & S_{22} & S_{23} & S_{24} \\ S_{31} & S_{32} & S_{33} & S_{34} \\ S_{41} & S_{42} & S_{43} & S_{44} \end{bmatrix} \begin{bmatrix} V_1^- \\ V_2^- \\ V_3^- \\ V_4^- \end{bmatrix} \tag{3.26}$$

where subscripts 1...4 correspond to the four ports of the model. The + superscript refers to the incoming waves at the slots and the - superscript denotes the reflected waves. For a general excitation of the structure, the even- and odd mode voltages

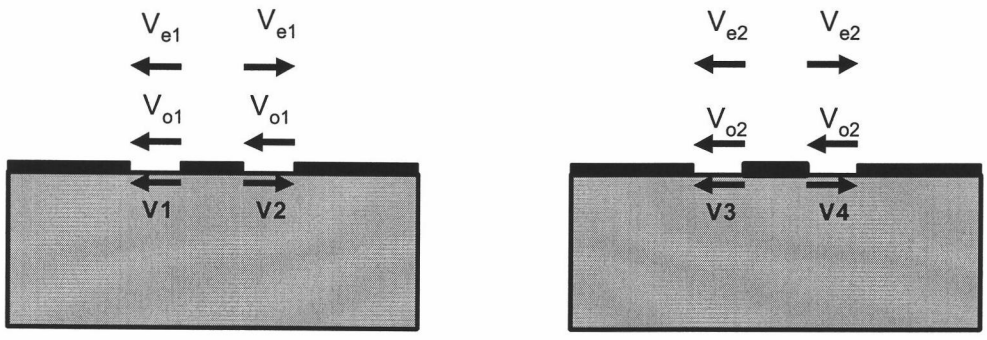

FIGURE 3.12. Slot exciations and modal voltages

can be expressed as a linear combination of the corresponding slot voltages. With reference to Fig. 3.12, the relationship between the modal voltages and slot voltages is given as

$$V_{o1} = \frac{V_1 - V_2}{2}$$

$$V_{e2} = \frac{V_3 + V_4}{2}$$

$$V_{o2} = \frac{V_3 - V_4}{2}$$

$$V_{e1} = \frac{V_1 + V_2}{2} \tag{3.27}$$

where subscripts $e1$ and $o1$ corresponds to the even- and odd modes on one side of the discontinuity, and $e2$ and $o2$ on the other side.

The above set of relations, when used in (3.26) gives a system of equations that relate the incoming and outgoing modal voltages at the four ports of the model.

$$V_{e1}^- = V_{e1}^+ \frac{(S_{11} + S_{12} + S_{21} + S_{22})}{2} + V_{e2}^+ \frac{(S_{13} + S_{14} + S_{23} + S_{24})}{2} \tag{3.28}$$

$$+V_{o1}^+ \frac{(S_{11} - S_{12} + S_{21} - S_{22})}{2} + V_{o2}^+ \frac{(S_{13} - S_{14} + S_{23} - S_{24})}{2}$$

$$V_{o1}^- = V_{e1}^+ \frac{(S_{11} + S_{12} - S_{21} - S_{22})}{2} + V_{e2}^+ \frac{(S_{13} + S_{14} - S_{23} - S_{24})}{2} \tag{3.29}$$

$$+V_{o1}^+ \frac{(S_{11} - S_{12} - S_{21} + S_{22})}{2} + V_{o2}^+ \frac{(S_{13} - S_{14} - S_{23} + S_{24})}{2}$$

Identical equations can be derived for the outgoing modal voltages V_{e2}^- and V_{o2}^- on the other side of the discontinuity. The first term in equation (3.28) is the reflection coefficient for the even mode. That is, for

$$V_{e2}^- = V_{o1}^- = V_{o2}^- = 0$$

we have

$$R_{ee} = \frac{V_{e1}^-}{V_{e1}^+} = \frac{(S_{11} + S_{12} + S_{21} + S_{22})}{2} \tag{3.30}$$

Applying similar definitions, equation (3.28) is re-written as

$$V_{e1}^- = V_{e1}^+ R_{ee} + V_{e2}^+ T_{ee} + V_{o1}^+ R_{eo} + V_{o2}^+ T_{eo} \tag{3.31}$$

Here, T_{ee} is the even-mode transmission coefficient, and R_{eo} and T_{eo} are the even-mode reflection and transmission coefficients, respectively, due to an incident odd mode.

The modal transmission and reflection coefficients describe the bend completely and are very useful in the analysis of the discontinuity. For example, the mode conversion in the bend can be directly observed by plotting the transmission coefficients T_{eo} and T_{ee} over the frequency range of interest. A high value of T_{oe} implies that more of the even-mode power is converted to the odd mode. The

magnitude of T_{ee} would understandably dip in a frequency band where T_{oe} peaks. Similarly, the odd-to-even mode conversion can be analyzed.

A general scattering matrix S_m, which relates the incoming and outgoing modal voltages at the discontinuity, is given by

$$\begin{bmatrix} V_{e1}^{+} \\ V_{e2}^{+} \\ V_{o1}^{+} \\ V_{o2}^{+} \end{bmatrix} = \begin{bmatrix} R_{ee} & T_{ee} & R_{eo} & T_{eo} \\ T_{ee} & R_{ee} & T_{eo} & R_{eo} \\ R_{oe} & T_{oe} & R_{oo} & T_{oo} \\ T_{oe} & R_{oe} & T_{oo} & R_{oo} \end{bmatrix} \begin{bmatrix} V_{e1}^{-} \\ V_{e2}^{-} \\ V_{o1}^{-} \\ V_{o2}^{-} \end{bmatrix} \tag{3.32}$$

This modal scattering matrix representation uses one port for each mode excited on either side of the discontinuity. The slot excitations are with reference to the port impedances Z_s. The modal scattering matrix is normalized to even- and odd mode impedances as given by the following set of equations [39].

$$Z = \sqrt{Z_t}(1 - S)^{-1}(1 + S)\sqrt{Z_t} \tag{3.33}$$

$$S_n = \sqrt{Y_n}(Z - Z_n)(Z + Z_n)^{-1}\sqrt{Z_n} \tag{3.34}$$

where

$$Z_t = \begin{bmatrix} Z_s & 0 & 0 & 0 \\ 0 & Z_s & 0 & 0 \\ 0 & 0 & Z_s & 0 \\ 0 & 0 & 0 & Z_s \end{bmatrix}$$

and

$$Z_n = \begin{bmatrix} Zo_e & 0 & 0 & 0 \\ 0 & Zo_e & 0 & 0 \\ 0 & 0 & Zo_o & 0 \\ 0 & 0 & 0 & Zo_o \end{bmatrix}$$

It should be noted here that equations (3.33) and (3.34) are valid only if Z_t and Z_n are diagonal matrices. In the above equations, Y_n is given by the inverse of Z_n,

S is the scattering matrix with reference port impedances Z_s and S_n is the modal scattering matrix renormalized to the even- and odd mode impedances.

3.6. Simulations and Results

A general technique to develop models for CPW bends was described in the earlier section. Specifically, model parameters were derived for right-angle and 45 degree bends. In this section, the models for these bends are compared with full-wave simulations. Right-angle bends with different s/w ratios have been considered here to provide a good variation in geometry. The dependence of the modal transmission coefficients on slot width s, center conductor width w, s/w ratio and the dielectric constant ϵ_r of the substrate is discussed.

3.6.1. Results for right-angled bends

To proceed with the analysis, a CPW right-angle bend with $w = 5$mm and the $s = 0.6$mm is considered. The dielectric substrate is assumed to be RT/Duroid [42] ($\epsilon_r = 2.33$) of thickness 62mil (1.58mm). The loss factor of the dielectric and the conductor thickness are assumed to be negligible. The bend was simulated with slot ports in the commercially available software tool MOMENTUM [31] to obtain a slot-voltage S-matrix. The slot-voltage S-matrix was then transformed to the modal S-matrix based on equations given in the previous section. An identical approach is adopted to extract the modal S-matrix from the bend model.

As emphasized earlier, a bend has two predominant effects on signal propagation in the CPW. First of all, it introduces a phase-shift between the signals in the two slots. This is the most significant factor in inducing mode conversion. Energy is transferred between the slots to offset the imbalance of power in the bend region.

Secondly, the coupling between the quasi-slot lines causes the even- and odd mode resonant frequencies to differ.

To analyze this behavior more thoroughly, let us consider the model for the CPW bend without the coupled-line section (a hypothetical structure). It

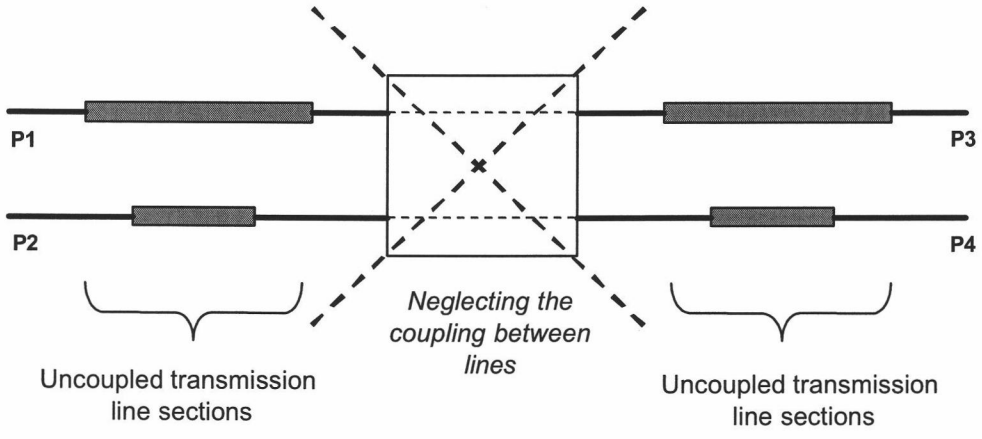

FIGURE 3.13. Modified Model

would just comprise the transmission line sections that account for the path-length difference between the slots in the bend. An illustration of this modified model is shown in Fig. 3.13. The port definitions here are assumed to be the same as that for the original model. The modal response of such a system would be as shown in Fig. 3.14 by the dashed lines. The even- and odd mode transmission coefficients (T_{ee}, T_{oo}) overlap and dip at 11GHz. In other words, the even-mode resonant frequency coincides with that of the odd mode. It is easy to see that there is no signal transmission between the diagonal ports (1, 4) and between (2, 3). The equations that were derived for transmission coefficients in the earlier section are accordingly modified to give

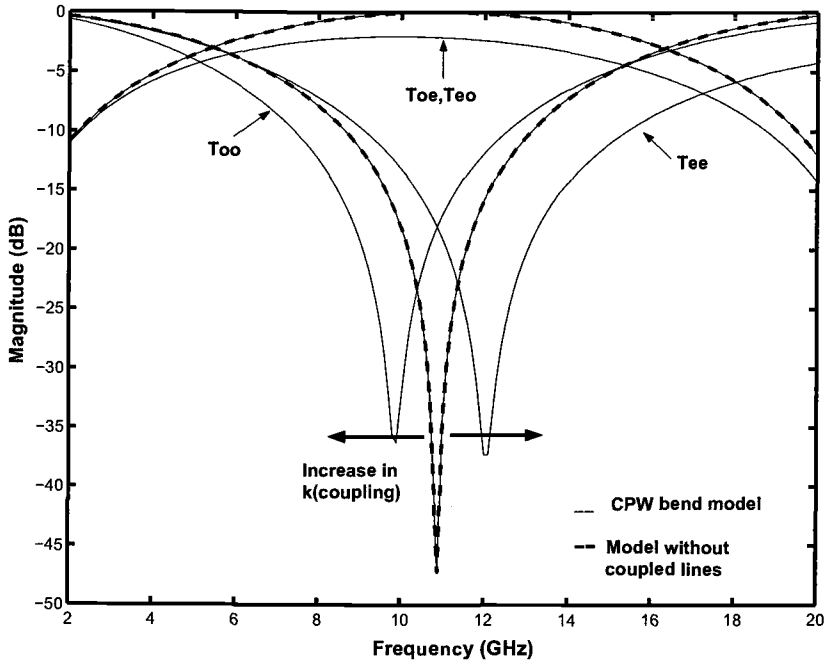

FIGURE 3.14. Modal transmission coefficients

$$S_{14} = S_{41} = S_{23} = S_{32} = 0$$

$$T_{ee} = T_{oo} = \frac{S_{13} + S_{24}}{2} \tag{3.35}$$

As seen in the above equation, the transmission coefficients for the even- and odd mode are equal. This explains the overlap in the two transmission coefficients at resonance. Now, if the coupled-line section is included, the transmission coefficients T_{ee} and T_{oo} show different resonant frequencies. This is in fact what occurs in the bend due to the coupling between the quasi-slot lines. There is a finite energy exchange between adjacent quasi-slot lines by means of coupling to give $S_{14} = S_{41} = S_{23} = S_{32} \neq 0$.

Now the right-angle CPW bend is considered in more detail. As discussed previously, the bend couples the slots more tightly than a straight coupled-line

section, and this effect is included in the model through the factor k. Figure 3.14 shows the variation of the even- and odd mode resonant frequencies with factor k. The higher the value of k, the greater the coupling and therefore, the larger the separation between the T_{ee} and T_{oo} 'dip' frequencies. The model was simulated in ADS [31] for varying values of k, and the response was compared with that obtained from MOMENTUM. It has been found that a value of $k = 1.6$ best models the actual coupling in the CPW bend. Figure 3.15. shows a plot of error in frequency-split (between the T_{ee} and T_{oo} resonant frequencies) versus the factor k. It is seen that the error is mimimum for a value of k ~1.55 to 1.6. Right-angle bends of different dimensions were studied, and it was ascertained that a value of 1.6 for k minimizes the error for most of the cases.

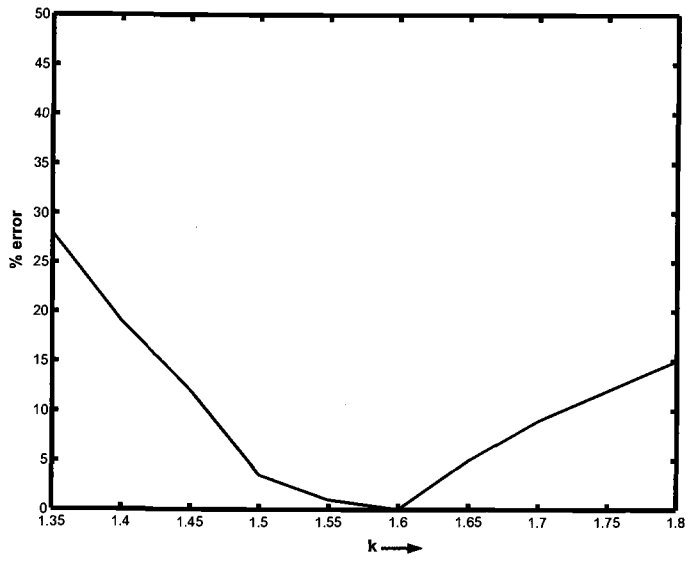

FIGURE 3.15. Variation of k

Figure 3.16 compares the modal transmission coefficients obtained from the model and MOMENTUM for a CPW right-angle bend with w=5mm, s=0.3mm.

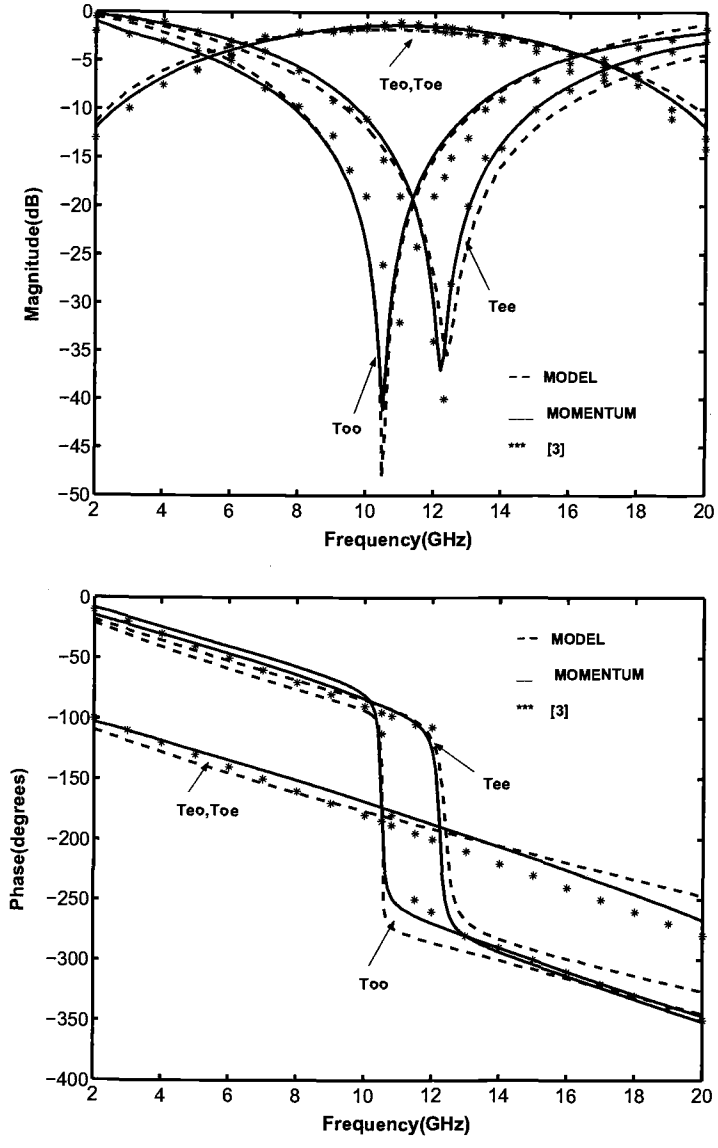

FIGURE 3.16. Modal transmission coefficients for a right-angle CPW bend (w=5mm, s=0.3mm, ϵ_r=2.33)

The results from reference [4] have also been included in the plot for comparison. There is a good match between the transmission coefficients obtained from the model and the other two sources. It is seen that the resonant frequencies for the even- and the odd modes occur at about 12GHz and 10.2GHz, respectively. The magnitude

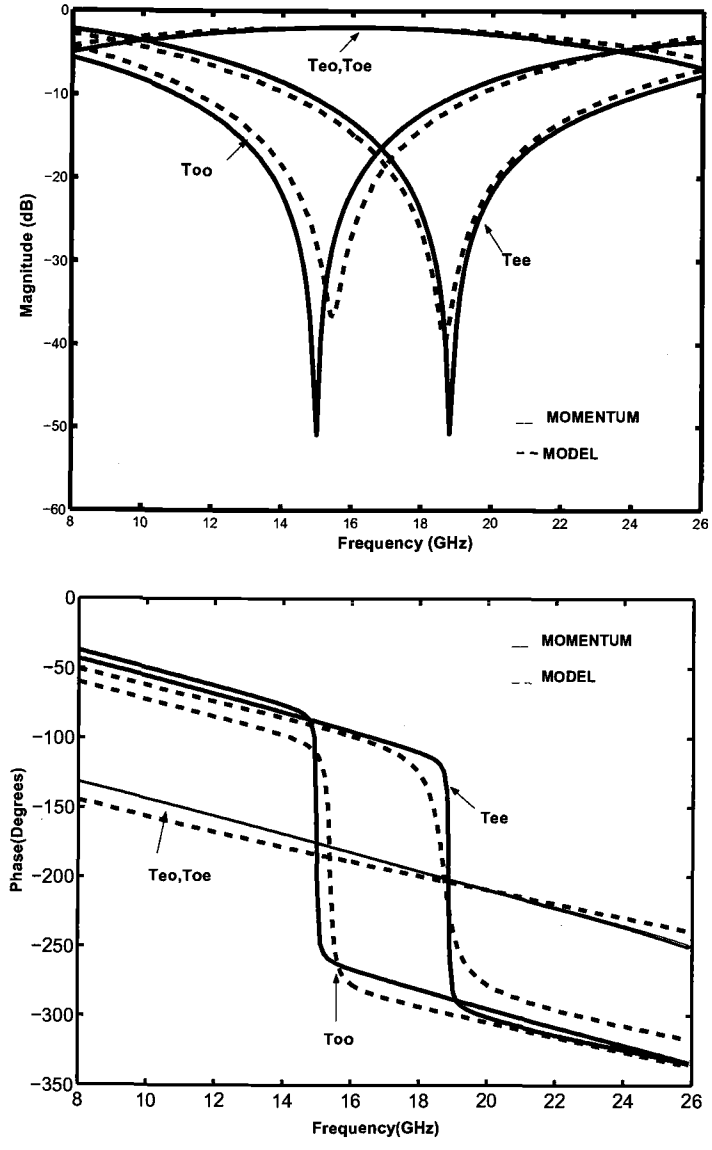

FIGURE 3.17. Modal transmission coefficients for a right-angled CPW bend (w=3mm, s=0.5mm, ϵ_r=2.33)

of the even mode transmission coefficient T_{ee} dips to its lowest value at 12GHz, signifying that most of the even-mode energy is converted to the odd mode at this frequency. As a result, the magnitude of T_{oe}, which represents the mode conversion

from even-to-odd mode, peaks in this frequency range. A similar argument explains the frequency behavior of T_{oo} and T_{eo}.

The modal transmission coefficients for another bend with dimensions $w =$ 3mm, $s = 0.5$mm and on the same substrate are shown in Fig. 3.17. The even- and odd mode resonant frequencies are at 19GHz and 15GHz, respectively, for this bend. The modal behavior is consistent with the theory that has been described. Once again, the model matches well with full-wave simulations, thus proving its validity.

3.6.2. Effect of geometry on mode conversion

The center conductor width w, and the slot width s, play an important role in determining the even- and odd mode resonant frequencies. The transfer of energy from one mode to the other takes place because of the path-length difference between the two quasi-slot lines. This comes directly from the relations between the slot voltages and the respective modal voltages. Complete mode conversion occurs, when the path-length difference between the two quasi-slot lines equals half a wavelength (180 deg). This is easy to see as, in this case the odd mode is anti-symmetric with respect to the even mode. Thus, the effect of changing w and s, correspondingly modifies the path-length difference shifting the even- and odd resonant frequencies shifts up or down the frequency spectrum. Shifting of even- and odd mode resonances to lower frequencies is usually undesirable, as most applications require a 'clean' transmission. The difference in the length of the two quasi-slot lines in the bend, is directly related to the center conductor width w and to a smaller extent on slot width s. Thus, it is better to have a wider bend or a CPW with smaller w when sharp bends are a necessity. The undesirable effects associated with mode conversion are then reduced or avoided in the frequency range of interest.

The difference in the even- and odd mode resonant frequencies is due to the coupling between the quasi-slot lines. Considering the relations for the modal transmission coefficients given in equations (3.28) and (3.29), it is seen that the transmission coefficients between diagonal ports, S_{14} and S_{23}, cause the split in the modal 'dip' frequencies. The closer the slots are, the stronger the coupling and, therefore the greater separation in the resonant frequencies.

From the above discussions, it becomes clear that the modal response of a right-angle bend in the CPW depends mainly on w. The slot width s does not have much of an effect on the frequency behavior of the transmission coefficients. However, it can contribute, albeit slightly, to the path-length difference in the bend.

3.6.3. Effect of dielectric substrate

The modal parameters of the coupled-line section such as the impedances and propagation constants depend on the properties of the substrate. The wavelength of the propagating modes in a dielectric has an inverse square relationship to the dielectric constant ϵ_r of the substrate. The electrical path-length difference between the two slots in the bend, is greater in terms of wavelength for a substrate with higher ϵ_r. The even- and odd mode resonances would then occur at lower frequencies, as the path-length difference corresponds to a 180 degree phase difference at lower frequencies. The converse hold true for bends with lower substrate ϵ_r.

The split in the even- and odd mode resonant frequencies is observed to be less for substrates with higher dielectric constant. The effects of the dielectric on the modal resonant frequencies is illustrated in Fig. 3.18. A right-angled bend in a CPW (w = 5mm, s = 0.3mm) has been considered here. The modal transmission coefficients for the bend were shown earlier for an RT/Duroid ($\epsilon_r = 2.33$) substrate. The resonant frequencies for T_{oo} and T_{ee} were found to be around 10.5GHz and 12GHz,

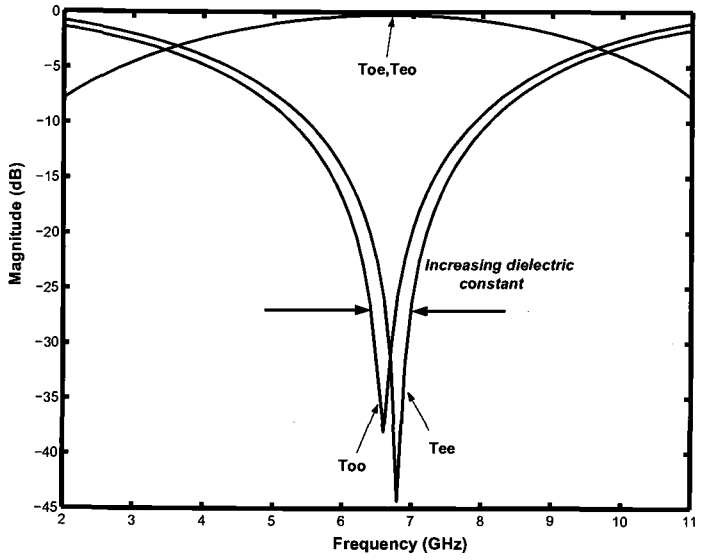

FIGURE 3.18. Modal transmission coefficients for a CPW bend (w=5mm, s=0.3mm, ϵ_r=9.6)

respectively, for RT/Duroid substrate. If the dielectric is changed to Alumina (ϵ_r = 9.6), the same bend would have the T_{oo} and T_{ee} dipping at 6.5GHz and 6.8GHz, respectively. The resonances now occur at lower frequencies when compared with a Duroid substrate. The coupling between the two quasi-slot lines is also weaker and, as a result, there is not much frequency difference in the modal 'dips'. The results obtained from the model were cross-checked with MOMENTUM, and an identical behavior was observed between the two.

3.6.4. Results for 45 degree bends

The modal transmission coefficients for a 45 degree bend are given in Fig. 3.19. The plots show the magnitude and phase comparisons of transmission coefficients obtained from the model and with MOMENTUM. Looking at the behavior of the even- and odd mode transmission coefficients, it is evident that the

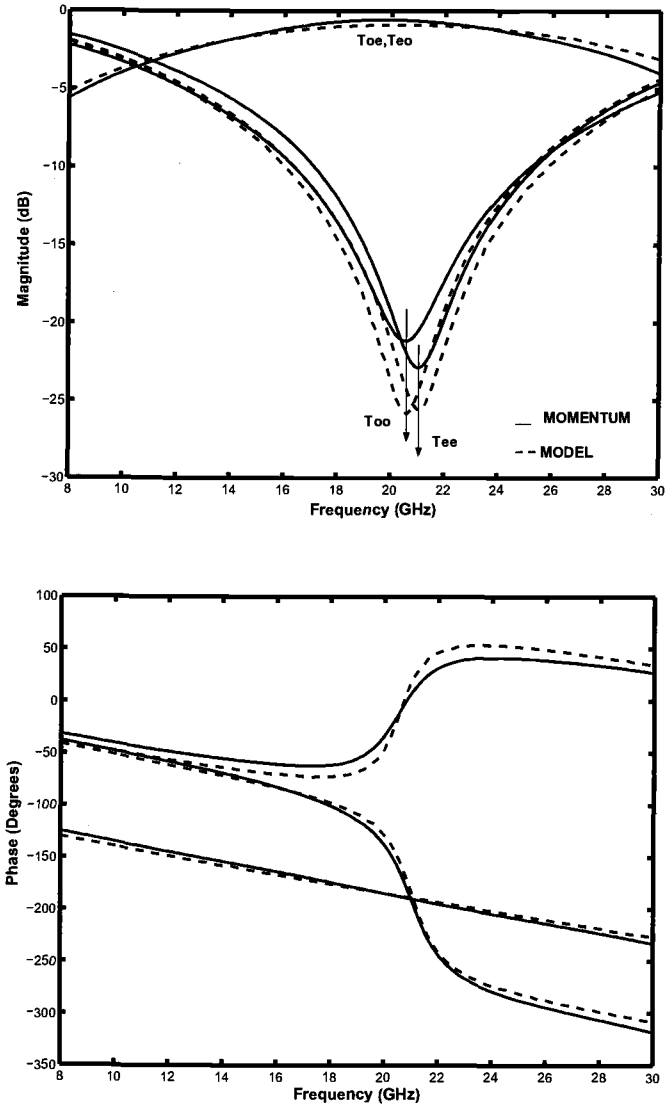

FIGURE 3.19. Modal Transmission Coefficients for a 45 degree CPW bend(w=6mm, s=1mm, ϵ_r=2.33)

coupling between the two slots is weaker than in a right-angle case. This is because, the electric fields begin to spread out when the angle of the bend starts decreasing from 90 degree. As a result, there is less overlap of fields in the bend region and therefore less coupling. The path-length difference between the slots is also lesser

in comparison to a right-angle case, thereby causing the modal resonances to occur at higher frequencies. Good agreement between model and MOMENTUM results proves the validity of the model.

3.7. Mitered Bends

Bends in transmission lines and waveguides are sometimes mitered, to smoothen sharp edges in the bends. This helps in minimizing reflections that deteriorate the energy handling capacity of the transmission line or waveguide. There are two popular techniques in mitering bends - mitering only the outer edge, or mitering both the outer and inner edges. The effects of mitering in microstrip bends have been studied extensively. Electromagnetic analysis has been performed to evaluate the characteristics of mitered microstrip bends in [43], [44]. Effects of mitering on CPW right-angle bends has been analyzed in [19]. However, simple models that can accurately predict the behavior of such bends are not available. This section deals with the modeling of mitered CPW right-angle bends - both single-sided and double-sided miters.

3.7.1. Modeling approach

3.7.1.1. Single-sided miter

Figure 3.20 shows a right-angle CPW bend with a 45 degree miter on the outer side. This structure can be modeled using the same procedure developed for non-mitered bends. With reference to earlier discussions, the model for the mitered bend consists of a coupled-line section that accounts for the coupling in the bend, and transmission line sections that introduce the path-length difference between the

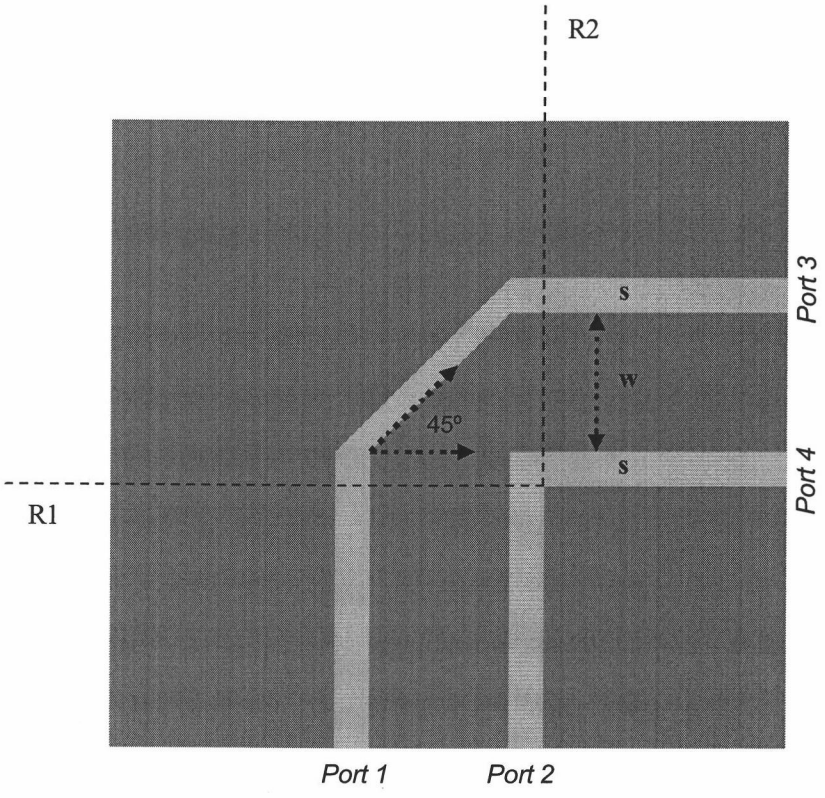

FIGURE 3.20. Single-sided mitered bend

slots. The length of the coupled-line section can be calculated by solving for the total mutual coupling between the quasi-slot lines. It turns out that the length is about a factor of $\sqrt{2}$ less than that for a non-mitered right-angle bend. However the value of coupling factor k that defines the modal impedances of the coupled-lines remains the same $k = 1.6$. The lengths of the transmission-line sections can be calculated from the geometry. The model parameters for the single-sided mitered bend are summarized below

$$\textbf{Coupled line length: } l_c = \frac{0.765}{\sqrt{2}} * (w + 2 * s) \tag{3.36}$$

$$\textbf{Coupling factor: } k = k_e = k_o = 1.6 \tag{3.37}$$

$$\textbf{Transmission line lengths: } l_{s1} = \frac{w + 1.297 * s}{\sqrt{2}}, l_{s2} = 0.5 * s \tag{3.38}$$

3.7.1.2. Double-sided miter

A right-angle CPW bend, which has a 45 degree miter on both the outer and inner slots, is shown in Fig. 3.21. This structure can be viewed as two continuous 45 degree bends, interposed by a uniform coupled-line section. The model for such a bend is also shown in the figure. The model parameters of the coupled lines that are sandwiched between two 45 degree bend sections can be assumed to be the same as that for the CPW lines feeding the bend. The parameters of the 45 degree bend model were given in equations (3.22) - (3.24). The lengths of the transmission line sections shown in Fig. 3.21 include contributions from both 45 degree bends. Hence,

$$l_{s1} = 2 * l_{s1(45)}, l_{s2} = 2 * l_{s2(45)} \tag{3.39}$$

where $l_{s1(45)}$ and $l_{s2(45)}$ are transmission-line lengths corresponding to each of the 45 degree bends.

3.7.2. Simulation and Results

Single- and double sided mitered bends were simulated in MOMENTUM and the modal transmission coefficients obtained were compared with those obtained from the respective models. A CPW bend that was considered earlier with w=5mm, s=0.3mm, and ϵ_r=2.33 has been modified here to include the mitering. Figure 3.22 shows the comparison between the model and MOMENTUM results for a single-sided mitered bend. The modal transmission coefficients for a double-sided mitered bend for the same w and s, and with l_u=2.5mm are shown in Fig. 3.23. There is

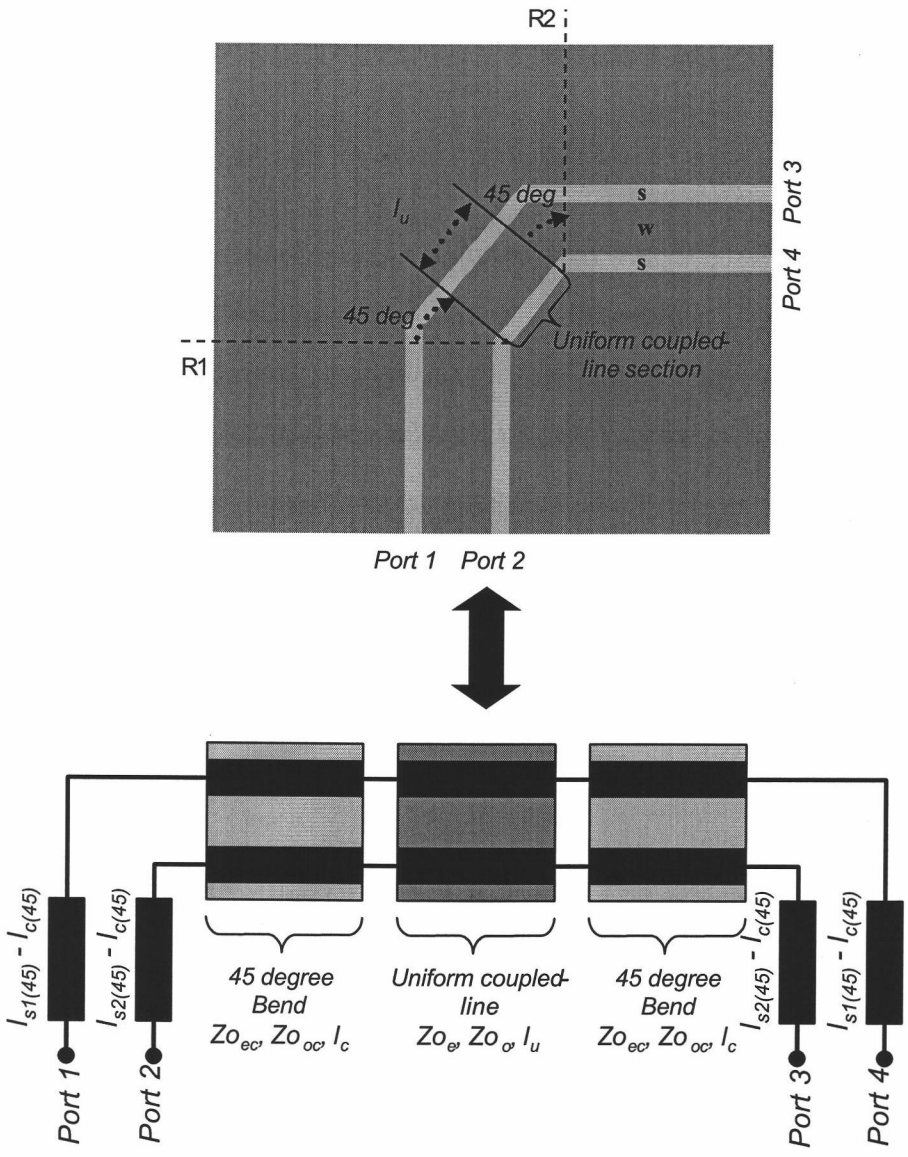

FIGURE 3.21. Double-sided mitered bend

a good match between full-wave simulations and the models over a wide frequency range, thereby proving the validity of the modeling approach.

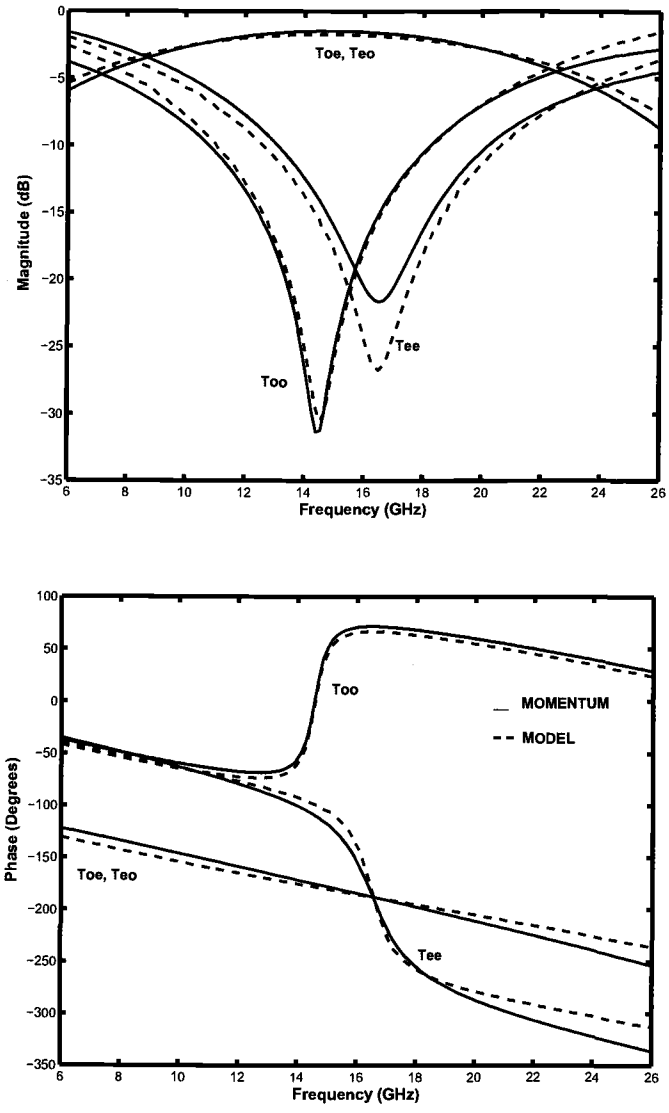

FIGURE 3.22. Modal Transmission Coefficients for a Single-sided mitered CPW bend (w=5mm, s=0.3mm)

3.7.3. Discussions

Mitering is a convenient technique to compensate bends in transmission lines by smoothing sharp edges to reduce reflections. The modeling methodologies for

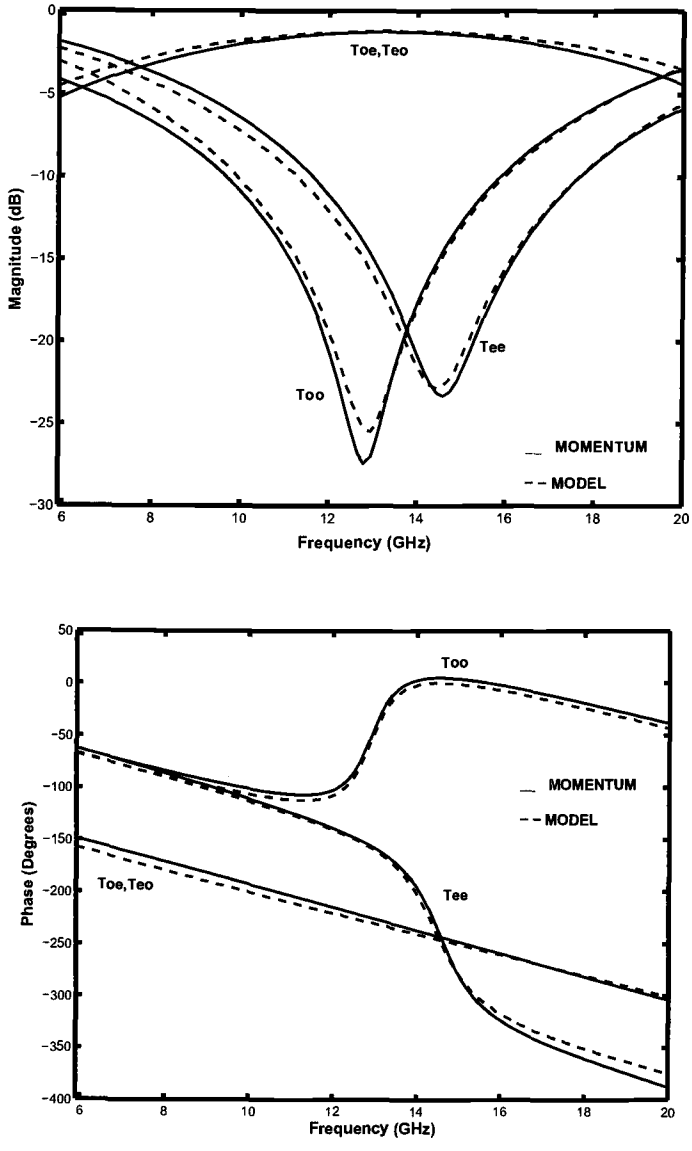

FIGURE 3.23. Modal transmission coefficients for a double-sided mitered CPW bend (w=5mm, s=0.3mm)

both these types of mitered bends were described in the previous section. While the model for the single-sided mitered bend uses the general theory that was developed in section 3.4, double-sided mitered bends are modeled as a cascade of two bend sections with coupled lines sandwiched between them.

Right-angle CPW bends with 45 degree single-sided and double-sided miters were modeled and the frequency response compared with full-wave simulations. It is obvious, that mitering of the right-angled bends pushes the even- and odd mode resonances up in the frequency spectrum. This is illustrated in Fig. 3.24. The shift in resonances to higher frequencies is because of the reduction in phase difference between the two slots due to mitering. This is desirable in many applications, in particular, in light of steadily increasing operating frequencies and signal bandwidths.

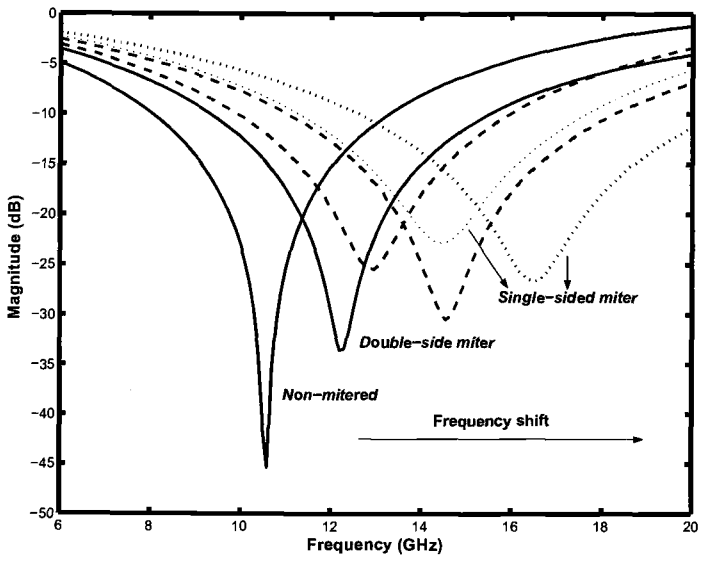

FIGURE 3.24. Effect of mitering on mode conversion: Modal transmission coefficients for a CPW right-angled bend (w=5mm, s=0.3mm, ϵ_r=2.33)

The modal 'dip' frequencies for a single-sided mitered bend, are higher than those for a double-sided miter. Furthermore, stronger coupling is observed between the slots in the single-sided mitered bend than in a double-mitered bend. This can be attributed to the sharper inner corner and closer proximity of the slots. As a

result, the even- and odd mode resonances are more widely spaced for a bend with single-sided miter.

Mode conversion in the double-sided mitered bend depends on the length l_u of coupled lines between the two bend sections. It is found that as l_u increases, the mode conversion becomes more subdued as shown in Fig 3.25. The 'dips' in even- and odd mode transmission coefficients (T_{ee}, T_{oo}) smoothen out and move up on the magnitude scale. This indicates a smaller percentage of energy in one mode is converted to the other around the resonance. Thus, a double-sided mitered bend with a higher l_u would be preferable, but at the cost of consuming greater board area.

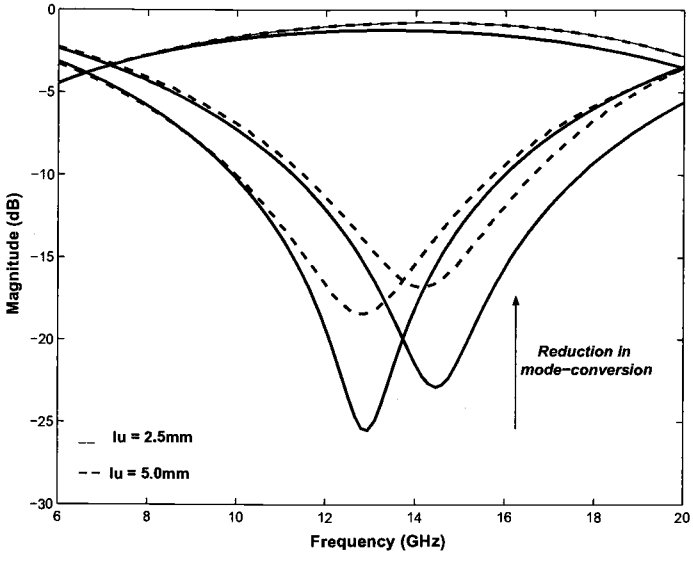

FIGURE 3.25. Effect of increasing l_u on mode conversion: Modal transmission coefficients for a CPW right-angled bend (w=5mm, s=0.3mm, ϵ_r=2.33)

3.8. Conclusion

Bends in the CPW have been analyzed as coupled quasi-slot lines, and a general modeling approach has been outlined for bends with varying angles and geometries. In particular, right-angle and 45 degree bends were studied and equivalent four-port models were developed for these bends. The results for modal transmission coefficients predicted by the models, match well with full-wave simulations for bends, with different w and s. It should be noted here that the model is based on the assumption that the CPW can be considered as a pair of coupled quasi-slot lines. This assumption, does not hold accurate for CPWs with relatively large s/w ratios. The error in the modal resonant frequencies between MOMENTUM and model increases with the s/w ratio. However, it has been found that for CPWs with s/w less than 0.25, the error is under 2% for right-angle bends.

Right-angle bends with 45 degree mitering at the outer edge, and bends with mitering at both outer and inner corners have also been modeled. Simulations have been done to study the behavior of mitered bends, vis--vis mode conversion. The mitered bends have been found to have a better performance compared to non-mitered bends. Mode conversion occurs at higher frequencies in mitered bends, which is desirable in RF/microwave and high-speed digital circuits.

4. CPW MEASUREMENTS

4.1. Network Analyzer Calibration

Microwave measurements were performed using a network analyzer. Network analyzers calculate S-parameters for the device under test (DUT) as ratios of complex voltage amplitudes. The general block diagram for the network analyzer measurement of a two-port device is shown in Fig. 4.1. The reference planes for such measurements is at some point within the analyzer. As a result, the measurement will include losses and phase delays caused by the effect of connectors, cables and transitions that must be used to connect the device under test (DUT) to the analyzer. In Fig. 4.1, these effects are lumped together, into two error boxes $E1$ and $E2$. They are placed between the reference planes of the DUT and the network analyzer ports.

The network parameters of the set-up includes the contributions from each of the blocks. The ABCD parameters of the system bounded by the reference planes of ports 1 and 2 is therefore a product of the ABCD parameters of individual blocks.

$$\begin{bmatrix} A_t & B_t \\ C_t & D_t \end{bmatrix} = \begin{bmatrix} A_{e1} & B_{e1} \\ C_{e1} & D_{e1} \end{bmatrix} \cdot \begin{bmatrix} A & B \\ C & D \end{bmatrix} \cdot \begin{bmatrix} A_{e2} & B_{e2} \\ C_{e2} & D_{e2} \end{bmatrix} \tag{4.1}$$

It is seen that the ABCD parameters offer a convenient way to compute the combined network parameters of multiple cascaded networks/components. The S-parameters of the cascaded systems, can then be easily obtained from ABCD parameters, knowing the reference port impedances.

In order to get the exact measurements for the DUT, the network parameters of the two error boxes $E1$ and $E2$ have to be calculated prior to measurements. The measurement results then need to be corrected to give the S-parameters of the DUT. In other words, the network analyzer should be calibrated prior to taking

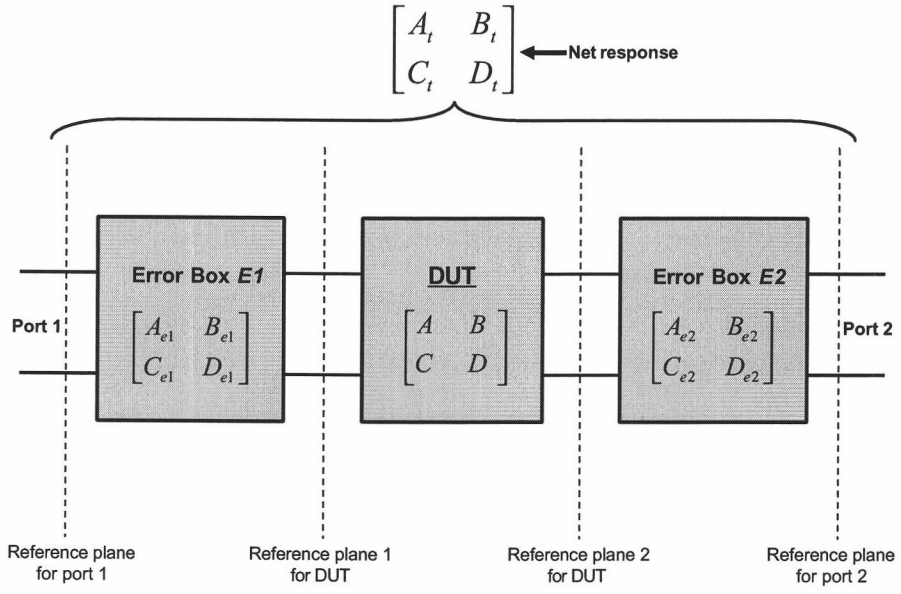

FIGURE 4.1. Block diagram for a two-port measurement setup

measurements. The general methodology for calibrating a network analyzer is to measure the response with known set of loads/standards, and to extract the error box coefficients from the measured response.

There are several calibration algorithms including Thru-Reflect-Line (TRL), Short-Open-load-Thru (SOLT), Line-Reflect-Reflect-Match (LRRM) and Short-Open-Load-Reciprocal (SOLR) etc. available for network analyzer measurements. Of the above mentioned, TRL and SOLT are perhaps among the most popular approaches. SOLT uses a set of standards provided by the manufacturer of network analyzers. TRL calibration requires a set of calibration standards to be fabricated by the user, and is most typically used when one wishes to remove artifacts from the measurement such as connector and probe discontinuities. Each of these methods have their advantages as discussed below.

The popularity of the SOLT calibration is due to the availability of calibration standards provided by the manufacturer of the network analyzer. This results in fabrication of fewer components and faster measurements. However, the zero phase (reference) point of the measurement is placed at the end of the connectors where the calibration was performed. Therefore, discontinuities, which occur after this reference point, can produce unwanted measurement artifacts.

Measurement artifacts introduced by connector and probe discontinuities can be negated by using the TRL calibration method. This requires the fabrication of calibration standards in the same configuration as the device that is to be tested. The standards used in the calibration are composed of a thru transmission line, a short or open and one or more delay lines. The thru transmission line is chosen to have the same impedance as that of the feed lines. The length of the line has to be adjusted such that it corresponds to the reference plane for the DUT. Therefore, the length should be chosen such that half the length of the thru line is shorter than the feeding line of the device under test.

The primary difference between the SOLT and TRL calibrations lies in where the reference planes are placed during measurement. A simple SOLT calibration, places the reference plane at the ends of the connectors attached to the network analyzer. This is undesirable, as the connectors to substrate discontinuities affect the measurement. But TRL calibrations, require the user to provide their own set of calibration standards. This technique places the reference plane into the DUT and calibrates out the connector or probe discontinuities.

While the measurement of straight DUTs can be performed in a straightforward manner, the measurement of orthogonal DUTs poses some calibration difficulties. This is mainly due to the fact that the orthogonal DUTs such as CPW bends are multi-moded in nature. There are undesired modes like the odd mode

that propagate in the device apart from the fundamental mode, for which the device is operated. These modes are not accounted for by the TRL and SOLT calibration methods. One approach to orthogonal measurements is to perform a straight calibration and carefully re-orient the probes prior to measurement. This step has to be performed very carefully using phase-stable cables to avoid measurement inaccuracies. An alternate measurement technique includes the use of SOLR calibration as explained in [30]. This type of calibration works around the requirement of a through standard, thus providing superior measurements for orthogonal DUTs compared to conventional techniques.

4.2. Theoretical Prediction of Measurement Response

The two-port S-parameter measurement response for the CPW bend can be predicted, knowing the 4x4 S-matrix for the bend. The modal S-matrix can in turn be derived from the slot-voltage S-matrix based on equations given in Chapter 3. The modal transmission and reflection coefficients that characterize the bend completely are then used to predict the measured response.

CPW measurements on printed-circuit boards (PCBs) are usually done using SMA connectors. The connectors short both ground conductors of the coplanar structure as illustrated in Fig. 4.2. This makes the connector almost a short for the odd mode, while it passes the even mode. The odd mode is thus reflected back-and-forth between the discontinuity and the connectors, forming a resonator-like structure. Figure 4.2 illustrates the effect of connectors on CPW measurements. The connectors are assumed to be placed at a distance l from the discontinuity.

At the discontinuity, the modal amplitudes for the incident and reflected waves for the odd mode will satisfy

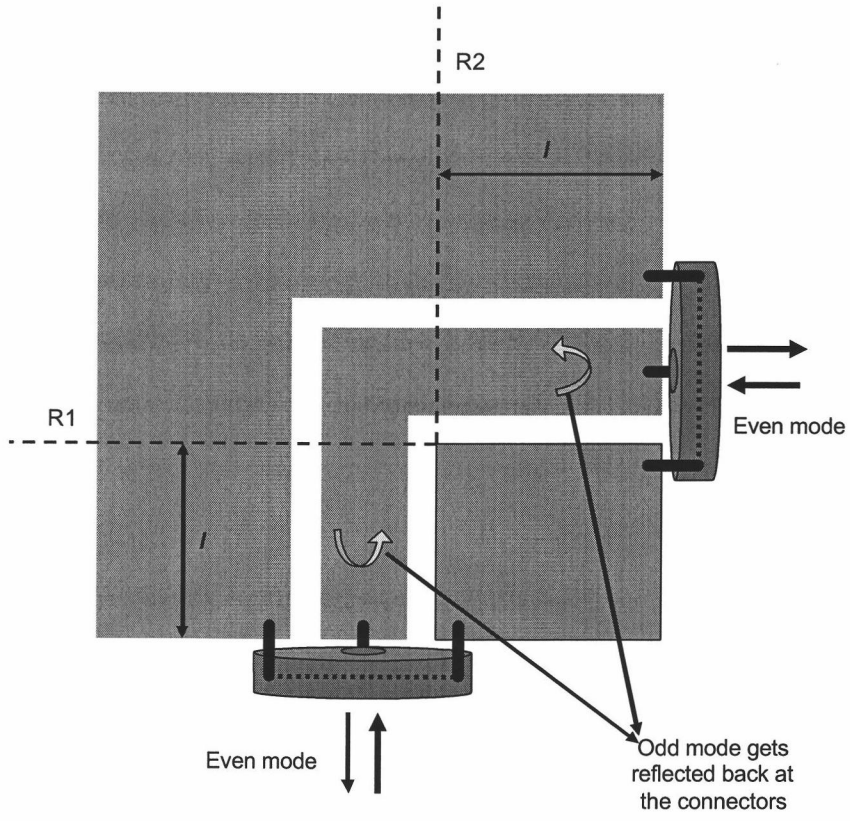

FIGURE 4.2. Effect of connectors

$$V_{o1,2}^{+} = -e^{-2\gamma_o d} V_{o1,2}^{-} \tag{4.2}$$

where

$$d = l + \Delta_c$$

Here, l is the length of the CPW feed lines, Δ_c is the extension length of the connector for the odd mode, and γ_o is the propagation constant for the odd mode that is obtained using quasistatic 2D methods. The extension length of the connectors, has been attributed to two factors - a quarter of the circumference of the connector's outer conductor and the equivalent length corresponding to the inductance of short-end discontinuity [4].

By using the above equation for the odd-mode reflection, the incident odd modes can be related to the incident even modes by

$$\begin{bmatrix} V_{1o}^{+} \\ V_{2o}^{+} \end{bmatrix} = - \begin{bmatrix} e^{-2\gamma_o l} + R_{oo} & R_{oo} \\ R_{oo} & e^{-2\gamma_o l} + R_{oo} \end{bmatrix}^{-1} \begin{bmatrix} R_{oe} & T_{oe} \\ R_{oe} & T_{oe} \end{bmatrix} \begin{bmatrix} V_{1e}^{+} \\ V_{2e}^{+} \end{bmatrix} \tag{4.3}$$

Eliminating the V_{1o}^{+} and V_{1o}^{+} terms in the set of equations, the two-port measured response is therefore given by

$$\begin{bmatrix} S_{11} & S_{12} \\ S_{21} & S_{22} \end{bmatrix} = \begin{bmatrix} R_{ee} & T_{ee} \\ R_{ee} & T_{ee} \end{bmatrix} - \begin{bmatrix} e^{-2\gamma_o l} + R_{oo} & R_{oo} \\ R_{oo} & e^{-2\gamma_o l} + R_{oo} \end{bmatrix}^{-1} \begin{bmatrix} R_{oe} & T_{oe} \\ R_{oe} & T_{oe} \end{bmatrix} \tag{4.4}$$

This gives

$$S_{11} = S_{22} = R_{ee} - R_{eo}A - T_{eo}B \tag{4.5}$$

$$S_{12} = S_{21} = R_{ee} - R_{eo}A - T_{eo}B \tag{4.6}$$

where

$$A = \frac{R_{oe}(1 + R_{oo}) - T_{oe}T_{oo}}{(1 + R_{oo})^2 - T_{oo}^2}, B = \frac{T_{oe}(1 + R_{oo}) - R_{oe}T_{oo}}{(1 + R_{oo})^2 - T_{oo}^2}$$

The two-port even-mode measurement response depends not only on the even-mode behavior, but also on the odd-mode characteristics and the distance of the connectors from the discontinuity. Due to reflections of the odd mode between the connectors and discontinuity, there is a resonator-like behavior for the odd mode that shows up in the measurement response. This distance l between the connectors and the bend, which also serves as the resonator length, plays an important role in determining the measured response. In the above derivation, the bend was assumed to be symmetric and the connectors to be soldered symmetrically on both sides of the discontinuity. Otherwise, the coupling between the even and odd modes at the connectors would also have to be considered in deriving the measured response.

4.3. Results

A CPW right -angled bend with w=3mm and s=0.5mm on RT/Duroid (ϵ_r = 2.33) substrate is considered. If the connectors are placed at a distance l=50mm from the discontinuity, the measured results at reference planes $R1$ and $R2$ can be predicted using equation (4.4). The magnitude and phase of S12 calculated from the model and MOMENTUM results are shown in Fig. 4.3. The ripples in the response, show the strong interaction that exists between the even and odd modes.

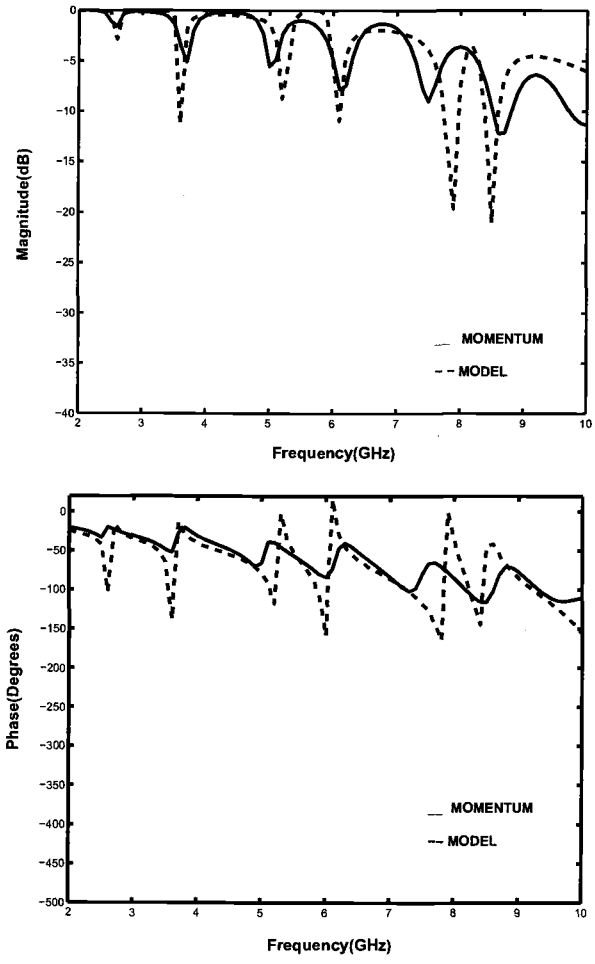

FIGURE 4.3. Predicted response (S12) at reference planes R1 and R2

It is obvious that mode-conversion significantly affects the frequency response of the bend.

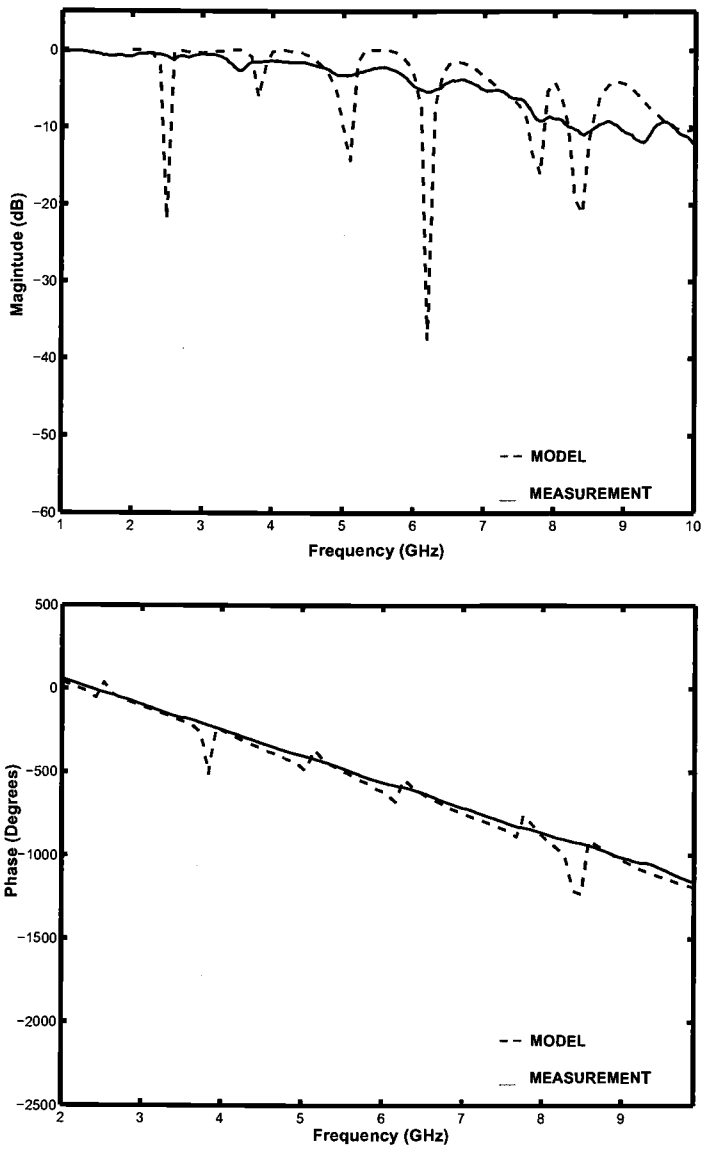

FIGURE 4.4. Predicted response (S12) at connectors

4.3.1. Experiments

A CPW right-angle bend with w=5mm, s=0.6mm and l=50mm was fabricated on RT/Duroid substrate for S-parameter measurements. The test fixture was terminated with SMA connectors and connected to an HP 8722C Network Analyzer. SOLT calibration was performed on the network analyzer before taking the S-parameter measurements. The measured response for S12 is shown in Fig. 4.4 along with the results from the model. It should be noted here that the reference planes for the ports are at the connectors. The connectors are of some finite length, which adds some extra phase to the measurement results. The extra phase addition is accounted for in the model by an extension length l_x=0.5mm used to adjust the length of the feed lines.

The agreement between the measured response and the model is good over most of the frequency range, as seen in Fig. 4.4. The deviation at certain frequencies can be attributed to the behavior of the connectors and soldering. The effects that connectors and soldering have on measurements are, however, not well understood. It is known, however, that they may affect the even and odd modes differently. Moreover, the substrate has some finite loss and is dispersive, whereas the model assumes an ideal lossless substrate.

4.3.2. Implementation in SPICE

The general model that has been developed for CPW bends consists only of transmission lines and ideal coupled line sections. The model can therefore be implemented in time-domain circuit simulators like SPICE. The four-port network model is modified to a two-port network for SPICE implementation. The quasi-slot lines are shorted at the ends, forcing an even-mode-only propagation. The

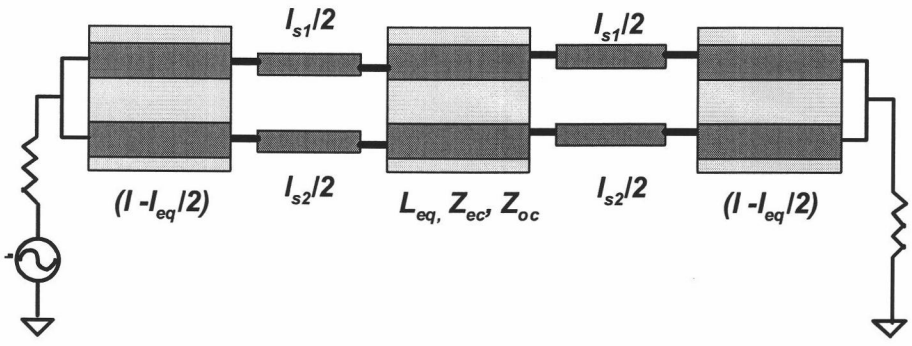

FIGURE 4.5. Implementation of the model in SPICE

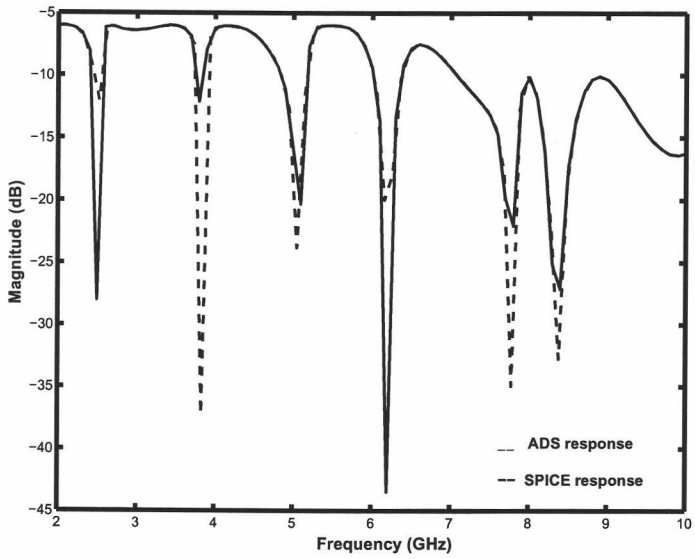

FIGURE 4.6. AC response in SPICE

response of this model comprises the modal interactions that take place at the bend discontinuity, while preserving two-port characteristics. Figure 4.5 shows a SPICE-implementable model for the test structure given in Fig. 4.2. The coupled lines in the model are modeled using the eigenmode description given in [45]. The netlist, given in Table A-1 in the appendix, was simulated in HSPICE [38]. Assuming an AC excitation of 1V and source impedance of 50 Ω, the frequency response at the

far end with 50 Ω terminations is shown in Fig 4.6. The response compares well with that obtained using ADS simulation, thereby proving the validity of the SPICE model.

4.4. Conclusions

An introduction to the basics of microwave measurements using network analyzers was given along with the calibration techniques that are most commonly used. The measured response of the bend discontinuity can be predicted, once the 4x4 modal S-matrix for the discontinuity is known. While the connectors are a thru for the even mode, they short the odd mode reflecting it back towards the discontinuity. The resultant measured response for the even mode has a strong contribution from the odd-mode standing-wave pattern that exists in the feed lines. The transmission response S12 of the bend is predicted using the modal S-matrices extracted from the model and MOMENTUM simulations. Comparisons are also shown between actual measured results for S12 and the model results for reference planes at connectors. Last, an implementation of the four-port model in SPICE has been presented along with the output AC response.

5. CONCLUSION AND FURTHER RESEARCH

5.1. Conclusion

A new approach has been presented in this thesis for modeling of bends in CPWs. The most attractive feature of this approach is its simplicity and the ease of obtaining model parameters. The frequency-dependent effects of the bend are illustrated clearly using coupled quasi-slot lines and single transmission lines in the model.

To start with, a brief introduction was given on CPWs, and the need for deriving simple models that characterize discontinuities was emphasized. The theory of multi-conductor transmission lines was discussed, followed by the procedure for extraction of transmission line parameters. The modal parameters of the CPW were then derived based on the application of multi-conductor theory to CPWs. Examples of common discontinuities were mentioned, along with the efforts and techniques adopted to study them in the past. Chapter 3 discussed the coupled transmission-line theory in brevity, leading to the analysis of CPWs as coupled quasi-slot lines. This discussion is important, as bends in CPWs are later modeled as a non-uniform coupled-line system.

Models were developed for right-angle bends, 45 degree bends, and mitered right-angle bends. The procedure for extracting the modal scattering matrix from general four-port slot excitations of the system was described. The results for modal transmission coefficients obtained from the model and full-wave simulations were then compared. Good agreement between the two results over a broad frequency range demonstrated the model's validity and accuracy. Effects of the bend geometry and substrate on mode conversion in the bend were then analyzed in detail. Chapter 4 discussed the basics of microwave measurements including calibration

techniques. The ill-effects of odd-mode excitation and mode conversion in the bend on measurements were highlighted. A comparison was shown between the actual measured response and model results. The thesis concluded with an insight on the implementation of the four-port model as a two-port system in SPICE.

5.2. Further Research

Suggestions for further research on the topic of this thesis are as follows. The models developed can be modified to include conductor and substrate loss effects, and certain frequency-dependent effects that may be significant at higher frequencies. This requires the modification of model parameters and the inclusion of lumped elements in the model. Besides, the extension of this modeling technique to coupled microstrips is a possibility, though lateral distributed effects have to be addressed here. There is also scope for the model to encompass conductor backed CPW (CB-CPW) discontinuities. Description of CB-CPW discontinuities, however, would require a more complicated six-port (three-mode) analysis of the system.

BIBLIOGRAPHY

[1] R.W. Jackson "Coplanar waveguide Vs. Microstrip for millimeter-wave integrated circuits " *IEEE MTT-S International Microwave Symposium Digest*, pp. 699-702, June 2, 1986.

[2] S. Ramo, J.R. Whinnery, T.V. Duzer, *Fields and Waves in Communication Electronics*, John Wiley and Sons Inc., New York 1994.

[3] K.C. Gupta, and A. Singh, *Microwave Integrated Circuits*, John Wiley and Sons Inc., New York 1974.

[4] M. Wu, S. Deng, R. Wu, and P. Hsu, "Full-Wave Characterization of the Mode-Conversion in a Coplanar Waveguide Right-Angled Bend" *IEEE Trans. Microwave Theory Tech.* vol 43, No. 11, pp. 2532-2538 Nov. 1995.

[5] N.I. Dib, M. Gupta, G.E. Ponchak, and L.P.B. Katehi, "Characterization of assymetric coplanar waveguide discontinuities " *IEEE Trans. Microwave Theory Tech.* vol 41, No. 9, pp. 1549-1558 Sep. 1993.

[6] R.W. Jackson, "Considerations in the use of coplanar waveguide for millimeter-wave integrated circuits" *IEEE Trans. Microwave Theory Tech.* vol 34, No. 12, pp. 1450-1456 Sep. 1986.

[7] N.I. Dib, L.P.B. Katehi, G.E. Ponchak, and R.N. Simons, "Theoretical and experimental characterization of coplanar waveguide discontinuities for filter applications" *IEEE Trans. Microwave Theory Tech.* vol 26, No. 5, pp. 873-882 May. 1991.

[8] N.I. Dib, L.P.B. Katehi, and G.E. Ponchak, "A theoretical and experimental characterization of coplanar waveguide shunt stubs" *IEEE Trans. Microwave Theory Tech.* vol 41, No. 1, pp. 38-44 Jan. 1993.

[9] K. Beilenhoff, H. Klingbeil, W. Heinrich and H.L. Hartnagel, "Open and short circuits in coplanar MMIC's" *IEEE Trans. Microwave Theory Tech.* vol 41, No. 9, pp. 1534-1537 Sep. 1993.

[10] L. Zhu "Realistic equivalent circuit model of coplanar waveguide open circuit: Lossy shunt resonator network" *IEEE Trans. Microwave and Wireless Components Letters* vol 12, No. 5, pp 1067-1072 May. 2002.

[11] N.I. Dib, G.E. Ponchak, and L.P.B. Katehi, "Analysis of shielded CPW discontinuities with air bridges" *IEEE MTT-S International Microwave Symposium Digest*, pp. 469-472, June 10-14, 1991.

[12] R. Schmidt and P. Russer, "Modeling of cascaded coplanar waveguide discontinuities by mode-matching approach" *IEEE Trans. Microwave Theory Tech.* vol 43, No. 12, pp. 2910-2917 Dec. 1995

[13] S. Mao, C. Hwang, R. Wu and C.H. Chen, "Analysis of coplanar waveguide-to-coplanar stripline transitions " *IEEE Trans. Microwave Theory Tech.* vol 48, No. 1, pp. 23-29 Jan. 2000.

[14] R.W. Jackson, "Excitation of the parallel-plate line mode at coplanar discontinuities" *IEEE MTT-S International Microwave Symposium Digest*, pp. 1789-1792, June 8-13, 1997.

[15] R.W. Jackson, "Mode Conversion at discontinuities in finite-width conductor-backed coplanar waveguide" *IEEE Trans. Microwave Theory Tech.* vol 37, No. 10, pp. 1582-1589 Sep. 1989.

[16] R.W. Jackson, "Mode-conversion at discontinuities in modified grounded coplanar waveguide" *IEEE MTT-S International Microwave Symposium Digest*, pp. 203-206, May 25-27, 1998.

[17] T. Becks and I. Wolff, "Full-wave analysis of various coplanar bends and T-junctions with respect to different types of air bridges" *IEEE MTT-S International Microwave Symposium Digest*, pp. 697-700, June 14-18, 1993.

[18] R.W. Jackson, "Excitation of the parallel-plate line mode at coplanar discontinuities" *IEEE MTT-S International Microwave Symposium Digest*, pp. 1789-1792, June 8-13, 1997.

[19] A.A. Omar, Y.L.Chow, L. Roy, and M.G. Stubbs, "Effects of air-bridges and mitering on coplanar waveguide 90 degrees bends: theory and experiment" *IEEE MTT-S International Microwave Symposium Digest*, pp. 823-826, Jun 14-18, 1993.

[20] J.J. Burke and R.W. Jackson, "Surface-to-surface transition via electromagnetic coupling of microstrip and coplanar waveguide" *IEEE Trans. Microwave Theory Tech.* vol 37, No. 3, pp. 519-525 Mar. 1989.

[21] W. Heinrich, "Quasi-TEM description of MMIC coplanar lines including conductor-loss " *IEEE Trans. Microwave Theory Tech.* vol 41, No. 1, pp. 45-52 Jan. 1993.

[22] R.W. Jackson, "Three-dimensional high-frequency distribution networks - Part I: Optimization of CPW discontinuities " *IEEE Trans. Microwave Theory Tech.* vol 48, No. 10, pp. 1635-1642 Oct. 2000.

[23] F. Alessandri, W. Menzel, M. Mongiardo and R. Sorrentino, "Efficient full-wave analysis of coplanar waveguide to slotline interconnections with finite metal-

lization thickness accounting for air brige effects" *IEEE MTT-S International Microwave Symposium Digest*, pp. 875-878, May 23-27, 1994.

[24] Y. C. Hahm, "Field theoretic analysis of a class of planar microwave and opto-electronics structure," *PhD Dissertation,* Department of Electrical and Computer Engineering, Oregon State University, Jan. 2000.

[25] D. Mirshekar-Syahkal, "Computation of equivalent circuits of CPW discontinuities using quasi-static spectral domain method " *IEEE Trans. Microwave Theory Tech.* vol 44, No. 6, pp. 979-984 Jun. 1996.

[26] C.P. Wen, "Coplanar waveguide: A surface strip transmission line suitable for nonreciprocal gyromagnetic device applications" *IEEE Trans. Microwave Theory Tech.* vol 17, No. 12, pp 1087-1090 Dec. 1969.

[27] J.B. Knorr and K. Kuchler, "Analysis of coupled slots and coplanar strips on dielectric substrate" *IEEE Trans. Microwave Theory Tech.* vol 21 pp. 594-596, Sep. 1973.

[28] M.E. Davis, E.W. Williams, and A.C. Celestini, "Finite-boundary conditions to the coplanar waveguide analysis" *IEEE Trans. Microwave Theory Tech.* vol 23 No. 7 pp 594-596, July 1975.

[29] H. Lee, "Computational methods for the quasi-TEM characteristics of fundamental MIC planar structures," *PhD Dissertation,* Department of Electrical and Computer Engineering, Oregon State University, Feb. 1983.

[30] S. Basu and L.Hayden, "An SOLR calibration for accurate measurement of orthogonal on-wafer DUTs" *IEEE MTT-S International Microwave Symposium Digest*, pp. 2532-2538, Nov 8-13, 1995.

[31] Agilent EEsof EDA, Santa Rosa, California, USA.

[32] M. Ribo, L. Pradell, "Circuit model for a coplanar-slotline cross" *IEEE Trans. Microwave and Guided Wave Letters.* vol 10, No. 12, pp. 511-513 Nov. 2000.

[33] W. Wiatr, D.K. Walker, and D.F. Williams, "Coplanar-waveguide-to-microstrip transition model" *IEEE MTT-S International Microwave Symposium Digest*, pp. 1797-1800, Jun 11-16, 2000.

[34] M. Ribo, L. Pradell, "Circuit model for mode conversion in coplanar waveguide assymetric shunt impedances " *Electronics Letters.* vol 35, No. 9, pp. 713-715 Apr. 1999.

[35] M. Ribo, J. Cruz, and L. Pradell, "Circuit model for mode conversion in coplanar waveguide assymetric series-impedances " *Electronics Letters.* vol 35, No. 21, pp. 1851-1853 Oct. 1999.

[36] M. Ribo, L. Pradell, "Model for cpw-to-slotline asymmetric transitions " *Electronics Letters.* vol 35, No. 14, Jul. 1999.

[37] D.P. Kasilingam and D.B. Rutledge, "Surface-wave losses of coplanar transmission lines" *IEEE MTT-S International Microwave Symposium Digest*, pp. 113-116, May, 1983.

[38] Star HSPICE, Avant! Corporation, Fremont, California, USA

[39] D.M. Pozar, *Microwave Engineering*, John Wiley and Sons Inc., New York 1998.

[40] P.C. Magnusson, G.C.Alexander, V.K.Tripathi, and A.Weisshaar, *Transmission Lines and Wave Propagation*, 4th edition, CRC Press, Dec 2000.

[41] R. Senguttuvan, L. Hayden, A. Weisshaar, "Mode-coupling in right-angled coplanar waveguide bends", *33rd IEEE European Microwave Conference*, Munich, Germany , Oct 6-10 2003.

[42] "RT Duroid 5880 data sheet" *Rogers Corporation, http://rogers-corp.com* .

[43] A.B. Broumas, H. Lino, and T. Itoh, "Transmission properties of right-angle microstrip bend with and without miter" *IEEE Trans. Microwave Theory Tech.* vol 37 No. 5, pp. 925-929 Apr 1989.

[44] J. Moore, and H. Lino, "Characterization of a 90 degree microstrip bend with arbitrary miter via the time-domain finite difference method" *IEEE Trans. Microwave Theory Tech.* vol 38 No. 4, pp. 405-410 Apr 1990.

[45] J.B. Rettig, and V.K. Tripathi, "A SPICE model for multiple coupled microstrips and other transmission lines", *IEEE Trans. Microwave Theory Tech.* vol 33 No. 12, pp. 1513-1518 Dec 1985.

APPENDIX

SPICE Netlist for the model

The model for the CPW bend with a finite length of feedlines was given in Fig. 4.5. The netlist for the model is given below in TABLE A-1. There are three coupled line sections in the model - one for the bend section at the center, and the other two to represent the CPW feedlines leading to the bend. The SPICE model for coupled lines given in [45] has been used here. This is preferred over the U-model in SPICE, because the latter may produce artifacts like ringing in the analysis of coupled transmission lines. The parameters of the individual coupled lines and transmission lines are obtained based on discussions in Chapter 3. The following netlist corresponds to a right-angle bend in the CPW with w=5mm, s=0.6mm and ϵ_r=2.33. The feedlines connected the bend are assumed to be identical on both sides and are of length l=50mm.

TABLE A-1

Parameter definitions:

.param m11=-0.7071 m12=0.7071 m21=0.7071 m22=0.7071

Input voltage source with source resistance:

Vin sour 0 ac=1v

Rin ipn sour 50

Termination on the other side:

Rout opn 0 50

CPW feedlines modeled as coupled-slotlines:

V1 1 5 0v

V2 2 7 0v

V3 3 11 0v

V4 4 9 0v

Voltage controlled voltage sources

E1 5 0 poly(2) a1 0 a2 0 m11 m12

E2 7 0 poly(2) a1 0 a2 0 m21 m22

E3 11 0 poly(2) a4 0 a3 0 m21 m22

E4 9 0 poly(2) a4 0 a3 0 m11 m12

Current controlled voltage sources

F1 0 a1 poly(2) v1 v2 m11 m21

F2 0 a2 poly(2) v1 v2 m12 m22

F3 0 a3 poly(2) v3 v4 m22 m12

F4 0 a4 poly(2) v4 v3 m11 m21

Uncoupled lines

T1 a1 0 a4 0 ZO=41.96 TD=217.56ps

T2 a2 0 a3 0 ZO=60.96 TD=231.50ps

Transmission lines accounting for the phase difference between the slots:

T3 4 0 p1 0 ZO=60.96 TD=44.18ps

T33 3 0 p11 0 ZO=60.96 TD=5.18ps

Coupled-lines for the bend:

V11 p1 51 0v

V21 p11 71 0v

V31 p22 111 0v

V41 p2 91 0v

Voltage controlled voltage sources

E12 51 0 poly(2) a11 0 a21 0 m11 m12

E21 71 0 poly(2) a11 0 a21 0 m21 m22

E31 111 0 poly(2) a41 0 a31 0 m21 m22

E41 91 0 poly(2) a41 0 a31 0 m11 m12

Current controlled voltage sources

F12 0 a11 poly(2) v11 v21 m11 m21

F21 0 a21 poly(2) v11 v21 m12 m22

F31 0 a31 poly(2) v31 v41 m22 m12

F41 0 a41 poly(2) v41 v31 m11 m21

Uncoupled lines

T11 a11 0 a41 0 ZO=27.98 TD=19.16ps

T21 a21 0 a31 0 ZO=90.294 TD=20.20ps

Transmission lines accounting for phase difference between the slots:

T4 p2 0 p3 0 ZO=60.96 TD=44.18ps

T44 p22 0 p33 0 ZO=60.96 TD=5.18ps

CPW feedlines modeled as coupled-slotlines:

V111 p3 511 0v

V211 p33 711 0v

V311 p44 1111 0v

V411 p4 911 0v

Voltage controlled voltage sources

E112 511 0 poly(2) a111 0 a211 0 m11 m12

E211 711 0 poly(2) a111 0 a211 0 m21 m22

E311 1111 0 poly(2) a411 0 a311 0 m21 m22

E411 911 0 poly(2) a411 0 a311 0 m11 m12

Current controlled voltage sources

F112 0 a111 poly(2) v111 v211 m11 m21

F211 0 a211 poly(2) v111 v211 m12 m22

F311 0 a311 ploy(2) v311 v411 m22 m12

F411 0 a411 poly(2) v411 v311 m11 m21

Uncoupled lines

T111 a111 0 a411 0 ZO=41.96 TD=217.56ps

T211 a211 0 a311 0 ZO=60.96 TD=231.60ps

Output statements:

.ac lin 100 50m 10g

.plot ac vdb(opn) vp(opn)

.options post

.end